UHF/VHF Antenna Design and Analysis for Automatic Deployable Emergency Beacons

by

Kalid A. Adem, **B.Eng**

A thesis submitted to the
Faculty of Graduate and Postdoctoral Affairs in partial
fulfillment of the requirements for the degree of

Master of Applied Science in Electrical Engineering

Ottawa-Carleton Institute for Electrical and Computer Engineering
Department of Electronics
Carleton University
Ottawa, Ontario
April, 2018

Abstract

In recent years, the disappearance of civilian aircraft such as the missing Malaysian Airlines MH370 and Air France AF447 fights has raised concerns amongst the public who could not accept the loss of their loved ones without clear evidence of what happened. Automatic Deployable Flight Recorders (ADFR) are designed to eject upon sensing a crash and transmit the location of the aircraft or crash while floating and protecting the black box recorder. The antenna unit residing within the ADFR must minimize the space it occupies while maximizing the usable radiated output power with minimal battery drain.

This thesis focuses on antenna designed for Cospas-Sarsat (C/S) first generation beacons at two frequencies of operations, 121.5 MHz and 406 MHz. A variant of an Alford-loop antenna was designed and shown to have a maximum gain of 2 dBi with an omnidirectional pattern in the horizontal plane while the concept of switching phase relationship of signals illuminating two vertically stacked loop antennas was demonstrated. A size reduction of about 50% was achieved by folding the corners of the loop while maintaining the current phase along the loop constant. Additionally, a novel horizontally polarized compact slotted-loop antenna was introduced using the theory of slots and loop antennas resulting in an omnidirectional pattern in the azimuth plane having a maximum gain of 1.8 dBi.

Acknowledgment

I would first like to thank my supervisor Dr. Jim Wight for taking me under his wings and giving me the opportunity to pursue this research, I am forever grateful. Jim, your guidance and support has been invaluable. I would also like to express my deepest gratitude to Dr. Aldo Petosa for steering me in the right direction in the early stages of this project and for finding the time to proofread this thesis.

I wish to acknowledge DRS Technologies for providing me the tools needed to make this research possible. Special thanks go to Joe Lostracco and Jim McKay for their guidance and support. Joe, you have been instrumental in helping me understand difficult concepts and I enjoyed all our technical conversations during the course of this work. Jimmy, you are the guru of everything RF and I am forever grateful for all the help you have given me in the anechoic chamber environment. Thank you to all my friends especially Jugraj Gill for your encouragement at times when I really needed it the most.

Most importantly, I want to thank my family, who never gave up on me and continued to be there for me. Your patience and understanding gave me the opportunity to pursue my dreams, without you this would not have been possible. My mother, who is the source of my strength and my father the reason I never lose faith, I am forever indebted to you. Lastly, to my uncle who has been an inspiration throughout my life, I want to express my sincerest appreciation for always being there and inspiring me to reach for the stars. I love you all.

Table of Contents

List of Tables

List of Figures

List of Acronyms

AUT	Antenna Under Test
ADFR	Automatic Deployable Flight Recorder
BAU	Beacon Airfoil Unit
BPSK	Binary Phase Shift Keying
CVR	Cockpit Voice Recorder
Cospas	Cosmicheskaya Sistyema Poiska Avariynich Sudov – (Russian for "Space System for the Search of Vessels in Distress")
C/S	COSPAS-SARSAT
EIRP	Effective Isotropic Radiated Power
ELT	Emergency Locator Transmitter
ELTM	Emergency Locator Transmitter Module
Galileo	European Global Satellite Navigation System
EUROCAE	European Organization for Civil Aviation Equipment
FGB	First Generation Beacon
FDR	Flight Data Recorder
GSA	Gain Standard Antenna
GEOSAR	Geostationary Orbiting Search And Rescue
GNSS	Global Navigation Satellite System
GPS	Global Positioning System
GLONASS	Globalnaya Navigazionnaya Sputnikovaya Sistema (Russian equivalent for GNSS)
IEEE	Institute of Electrical and Electronics Engineers
ICAO	International Civil Aviation Organization
LHCP	Left Hand Circular Polarization
LUT	Local User Terminal

LEOLUT	Low Earth Orbiting Local User Terminal
LEOSAR	Low Earth Orbiting Search And Rescue
MEOSAR	Medium Earth Orbiting Search and Rescue
MCC	Mission Control Centre
OQPSK	Offset Quadrature Phase-Shift Keying
PLF	Polarization Loss Factor
RTCA	Radio Technical Commission for Aeronautics
RHCP	Right Hand Circular Polarization
SAR	Search and Rescue
Sarsat	Search and Rescue Satellite-Aided Tracking
SGB	Second Generation Beacon
SPDT	Single Pull Double Throw
UHF	Ultra High Frequency
VHF	Very High Frequency
VSWR	Voltage Standing Wave Ratio

Chapter 1

1.1 Motivation

The detection and location of an aircraft's crash site is extremely important to potential survivors and for SAR teams to locate them in a timely manner. Studies show that while the initial survivors of an aircraft crash have less than a 10% chance of survival if rescue is delayed beyond two days, the survival rate is increased to over 60% if the rescue can be accomplished within eight hours [1]. For this reason, Emergency Locator Transmitters (ELTs) are required for most general aviation aircraft, boats, ships and individuals in distress that require assistance of rescue personnel. There is growing concern among the airline industry about the safety of air travel after the recent disappearance of Malaysian Airlines Flight 370 (MH370) in the Indian Ocean. This has encouraged regulators to apply robust regulations on standards guiding aircraft tracking. The solution was to improve detection probability and location accuracy by modernizing and deploying more satellites in the Medium Earth Orbit Search and Rescue (MEOSAR) to reduce delays of distress alerts [2]. COSPAS/SARSAT (C/S) is that international body which overlooks and maintains satellite networks that track aircraft in real time. All large commercial aircraft are mandated to have Cockpit Voice Recorders (CVR) and Flight Data Recorders (FDR), one in the nose section of the aircraft and one in the tail section for redundancy. The CVR captures conversations between pilots and radio communications while also recording engine noises in the cockpit. The FDR monitors fight parameters such as altitude, air speed and heading.

Many aircraft manufacturers, such as Airbus, have taken the initiative to implement these standards mandated by the International Civil Aviation Organization (ICAO) [Annex 6 and 10] in order to have aircraft location tracking in case of an incident. The Automatic Deployable Flight Recorder (ADFR) is one such solution currently being implemented. The

ADFR beacon unit is the device that flies away much like a frisbee. It will be mounted on the tail of the aircraft and upon impact it will deploy and fly away until it hits the ground or floats in ocean water. This is basically an ejectable 'black box' found in the tail of an aircraft in addition to the fixed black box found in the cockpit. When aircraft sensors detect the start of a crash, the ADFR releases from the aircraft and flies on its own until it lands in water or land at which time the transmitter in the ADFR unit starts transmitting, at 406 MHz through the integrated antenna, the location of the ADFR and identification of the host aircraft to satellites in orbit and relayed to international SAR authorities. For position information purposes, the ADFR is capable of receiving GPS, Galileo and GLONASS signals which is mandated by the ICAO for a commercial aircraft in distress. Airbus plans to take out the ELT and recorders in the tail section and replace them with an ADFR, which is expected to be operational by 2019 [3]. Figure 1 shows the steps of the ADFR recovery process.

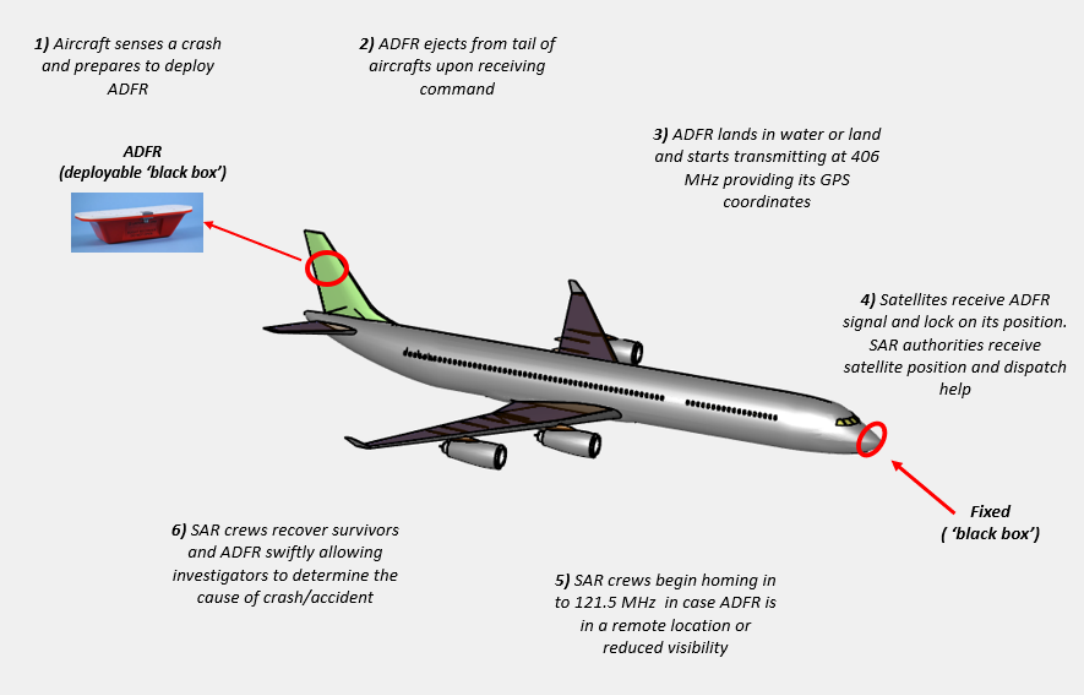

Figure 1: Recovery process of ADFR after deployment

The antenna unit is a critical component in the ADFR and must be compact and efficient in order to minimize the required space and power requirements. The antenna must be able to generate radio waves with sufficient intensity, and proper polarization, in order to be received and identified by satellites in the system and detected by ground stations in order to have search and rescue dispatched in the shortest time possible. The antenna has to also be crash survivable such that it can withstand severe crash impact forces. The antenna is a critical component of the deployable system. This research targets the design of small, compact and efficient antennas to be applied in vehicles operating in air, land and sea. There have been recent activities on designing distress antennas, however not a lot has been done on antennas for civilian aircraft, where it is required to have robust designs to meet harsh environments and satisfy C/S standards.

1.2 Thesis Purpose

The purpose of this thesis is to introduce a novel antenna design developed to meet demanding physical and electrical performance requirements of the ADFR for long range aircraft that employ deployable emergency beacons such as the Airbus A321LR, A330, A350 XWB, and A380. The deployable beacons consist of a transmitter operating at 406 MHz, 121.5 MHz and/or 243 MHz meeting First Generation Beacons (FGB) requirements mandated by Cospas-Sarsat (C/S T.001). For Second Generation Beacons (SGBs), the ELT must be compatible with specifications by C/S T.018, which is currently being defined by the C/S, EUROCAE and RTCA working groups. This thesis describes the design and development of the 121.5 MHz and 406 MHz antenna units for possible application in the ADFR adhering to FGB requirements. The antenna development is in its final stages with several advanced prototypes being produced for final evaluation in real beacon airfoil.

1.3 Thesis Contribution

Thesis contributions towards knowledge in antenna design are listed below:

- A review of electrically small passive antennas in the UHF and VHF band
- A design of folded slot antenna in the VHF band
- A design of an Alford-loop type antenna
- A novel design of a small and compact slotted-loop antenna using the principles of slot radiators as half-wavelength resonators.

1.4 Thesis Organization

This thesis is organized in five chapters. A brief description of what each chapter contains is presented below. Chapter 1 is the introduction section and briefly presents the motivation behind this research, purpose and contributions of the thesis towards the design and analysis of antennas for deployable beacons. Also, some background information on deployable emergency beacons is presented including the antenna requirements set by C/S T.001 and ED-62A/DO-180A. Chapter 2 presents fundamental knowledge required to understand and design antennas. Some of the topics covered include radiation pattern, directivity, polarization, and Voltage Standing Wave Ratio (VSWR). Chapter 3 and 4 presents UHF/VHF antenna solutions for the application in deployable beacons. Several antennas were surveyed with different geometries and compared with simulation results. Chapter 5 presents a summary of the work done and provides opportunity for future work including alternative methods to combine passive antenna elements to a host structure, the end result being maximum power transmission.

1.5 Antenna Requirements

The requirements for the UHF (406 MHz) and VHF (121.5 MHz) frequency bands are different in nature. The UHF antenna needs to fulfil the requirements imposed by C/S T.001 [4], in order to be compatible with C/S standard. For all azimuth angles and for elevation angles between 5^0 and 60^0, the antenna must have a hemispherical radiation pattern, with gain between -3 dBi and 4 dBi in 90 % of this region. The polarization can either be circular or linear. The VSWR needs to be smaller than 1.5:1 for the 406-406.1 MHz band. This corresponds to a reflection coefficient (S11) lower than -14 dB. This condition is stricter than the generally accepted standard, which is to obtain an S11 < -10 dB. Table 1 shows the tabulated requirements for 406 MHz antenna transmission according Cospas-Sarsat.

Table 1: Minimum requirements for 406 MHz antenna based on C/S T.001 (FGB)

Antenna Parameters	**Antenna Characterization**	**Comments**
Frequency	406 MHz	-
Radiation Pattern	Hemispherical	Omnidirectional radiation pattern in azimuth
Polarization	Linear or RHCP	Vertical/Horizontal or Right Hand Circular Polarized
Antenna Gain (Azimuth)	-3 dBi to +4 dBi	Over 90% of full 360^0 azimuth range
Antenna Gain (Elevation)	-3 dBi to +4 dBi	Over 90% of elevation range between $5^0 < EL < 60^0$
VSWR	≤ 1.5:1	50 Ω system

In real life applications in which the antenna will be used, there could be environmental conditions which can cause a shift in the resonance frequency. Therefore, it is always best to over design the antenna by accounting for safety margin. The VHF antenna needs to comply with ED-62A/DO-180A requirements [5], [6] which is the minimum operational performance requirement for ELTs. The minimum power output should be of greater than 50 mW Effective Isotropic Radiated Power (EIRP) for a 48-hour period transmitted by the ELT. Subsequent to this, for a further 102 hours, the 121.5 MHz ELT transmitter should transmit with a minimum output EIRP of 5 mW to assist in beacon homing and location. Details are summarized in Table 2.

Table 2: Minimum requirements for 121.5 MHz antenna

Antenna Parameters	**Antenna Characterization**	**Comments**
Frequency	121.5 MHz	-
Radiation Pattern	Omnidirectional radiation pattern in azimuth	Within 3 dB of four equally spaced azimuth angles
EIRP maximum	23 dBm (400 mW)	-
EIRP minimum	17 dBm (50 mW)	-

Chapter 2

2.1 Antenna Fundamentals

The main purpose of an antenna is to radiate electromagnetic waves through space, therefore it is imperative to determine how these radiated waves are transmitted and received when designing an antenna. Important antenna performance parameters such as, radiation pattern, directivity, gain, polarization, impedance, bandwidth and efficiency are used to characterize an antenna's suitability for a certain application. The following parameters are defined to characterize antennas introduced in this thesis and to better understand the challenges presented to antenna designers in the UHF/VHF band.

2.1.1 Radiation Pattern

IEEE defines radiation pattern as:

"…the spatial distribution of a quantity that characterizes the electromagnetic fields generated by an antenna". [7]

Typical characteristics used are power flux density, radiation intensity, directivity, phase, polarization, and field strength. The variation of the power radiated by an antenna is given as a function of the angles θ (elevation plane), ϕ (azimuth plane) at a fixed distance. The antenna is positioned at the origin of the spherical coordinate axis as in Figure 2.

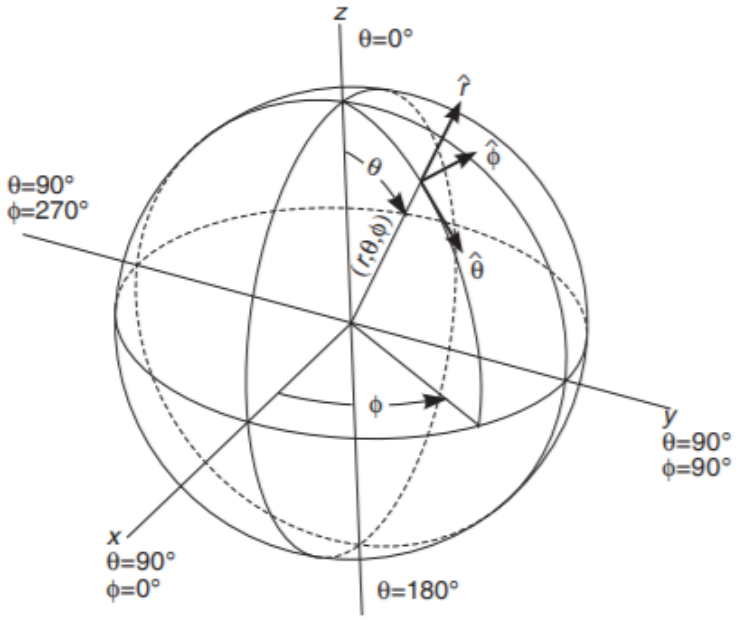

Figure 2: Spherical coordinates **[8]**

Depending on the application it may be desirable to have an antenna with a certain type of radiation pattern. An omnidirectional radiation pattern is one type in which the pattern is mostly a constant value or non-directional in a given plane and directional in the orthogonal plane. An isotropic antenna is the ideal omnidirectional antenna that radiates its power equally in all directions, and often used as a reference antenna for measuring antenna gain. Real antennas are always directional in at least one plane. Omnidirectional antennas are used in applications in which the direction of the signal transmission is unknown. An example of an omnidirectional radiation pattern is shown in Figure 53.

2.1.2 Directivity and Gain

IEEE defines directivity as "the ratio of the radiation intensity in a given direction from the antenna to the radiation intensity averaged over all directions. The average radiation intensity is equal to the total power radiated by the antenna divided by 4π". [7]

The average radiated power from an antenna is obtained by integrating the average radiated power density, W_{avg}, given as:

$$W_{avg} = \frac{1}{2} Re[E \times H^*] \tag{1}$$

The average radiated power, P_{avg}, is then given by the following expression:

$$P_{avg} = \frac{1}{2} \iint Re\ (E \times H^*) \cdot ds \tag{2}$$

where E and H are the radiated electric and magnetic fields, respectively, integrated over the entire closed spherical surface of the average power density. Radiation intensity, $U(\theta, \phi)$, is a far-field approximation and is simply the average radiation density scaled by the square product of the distance defined by [9] as, "the power radiated from an antenna per unit solid angle". It is expressed as:

$$U(\theta, \phi) = r^2 \cdot\ W_{avg} = \frac{1}{2} Re\ [E \times H^*] \cdot r^2 \tag{3}$$

To determine the total radiated power, P_{rad}, the radiation intensity, $U(\theta, \phi)$, is integrated over the entire solid angle. Thus:

$$P_{\text{rad}} = \iint U\ d\Omega = \iint sin\theta\ d\theta\ d\phi \tag{4}$$

where $d\Omega$ is the element of solid angle measured in steradians.

Given the radiation intensity, it can mathematically be shown that the directivity, $D(\theta, \phi)$, is the ratio of the radiation intensity in a given direction to the radiation intensity of an isotropic source, U_o, from all direction:

$$D(\theta,\phi) = \frac{U(\theta,\phi)}{U_o} \tag{5}$$

where the radiation intensity of an isotropic source is given as:

$$U_o = \frac{P_{rad}}{4\pi} \tag{6}$$

The maximum directivity, D_{max}, is expressed as:

$$D_{max} = \frac{U_{max}}{U_o} \tag{7}$$

where U_{max} is the maximum radiation intensity in a given direction.

The antenna gain G is related to the average directivity D and to the radiation efficiency, η, of an antenna [9] as

$$G\ (\theta,\phi) = \eta \cdot D\ (\theta,\phi) \tag{8}$$

The antenna gain is usually expressed in dBi and signifies the ratio of radiated power in a given direction (θ,ϕ) relative to that of an isotropic radiator which is radiating the electrical power uniformly in all directions. Based on IEEE standards, gain does not include losses arising from impedance and polarization mismatches [7]. The term realized gain is used when mismatch effects are included.

2.1.3 Radiation Efficiency

The radiation efficiency, η, is the ratio of directivity to gain. It takes into consideration all the power lost before radiation. The losses may be due to mismatch at the input terminals, and dissipative losses. It is also the ratio of P_{rad} to power accepted at the antenna input terminal in transmit mode, P_o. That is,

The definition by IEEE states the radiation efficiency as

> "…the radiation of the total power radiated by an antenna to the net power accepted by the antenna from the connected transmitter" [7]

That is:

$$\eta = \frac{P_{rad}}{P_o} = \frac{G\ (\theta, \phi)}{D\ (\theta, \phi)} \tag{9}$$

An efficient antenna radiates most of the input power yielding efficiency close to unity. An inefficient antenna has more of the power absorbed as losses within the antenna such as conduction losses, dielectric losses and spillover losses.

The total efficiency of an antenna, η_{total}, is the radiation efficiency multiplied by the impedance mismatch loss $(1 - |\Gamma|^2) \times \eta$ of the antenna. That is

$$\eta_{total} = (1 - |\Gamma|^2) \times \eta \tag{10}$$

The efficiency for small and compact antennas varies but is typically between 0.5 and 0.7.

2.1.4 Polarization

The polarization of an antenna is determined by the electric field in the direction where the field strength is a maximum. Polarization is achieved when the electric field and the magnetic field are perpendicular to each other and to the direction the plane wave is propagating. If vertical and horizontal elements in the same plane are fed out of phase (where the beginning of the RF period applied to the feed point of the vertical element is not in time phase with that applied to the horizontal), the resultant polarization is elliptical. Circular polarization is a special case of elliptical polarization and can be either right hand circular or left hand circular. The wave front of a circularly polarized signal appears (in passing a fixed observer) to rotate between vertical and horizontal, making a complete 360o rotation once every period. Aside from the type of polarization, two main factors are taken into consideration when considering polarization of an antenna, axial ratio and polarization loss factor, which can be referenced in [10], [11], [12], and [9].

2.1.5 Equivalent Isotropic Radiated Power (EIRP)

EIRP is the power produced by a perfect isotropic antenna that is the same as an antenna with its maximum gain at a given direction. It is the sum of the radiated power (P_R), and the gain (G) of the antenna at the input terminal [13]:

$$EIRP = P_R\,[dBm/dBW] + G\,[dB] \tag{11}$$

EIRP is often specified for the transmit antenna to allow designers trade-off between available power and antenna gain in order to meet requirements.

2.1.6 Voltage Standing Wave Ratio (VSWR)

In a normal configuration, antennas are powered by a transmitter through a cable or transmission line. If the antenna impedance does not match to the characteristic impedance of the cable, maximum power will not be received by the antenna. If a sinusoidal signal is travelling down the transmission line towards the antenna, an impedance mismatch between the cable and the antenna will cause the sine wave to propagate back up the cable in the reverse direction toward the transmitter causing the signals to constructively and destructively interfere. The ratio of maximum to minimum voltage of the standing wave is the VSWR and is given as:

$$VSWR = \frac{1 + \Gamma}{1 - \Gamma} \tag{12}$$

where Γ describes the voltage reflected from the antenna. A VSWR of 1:1 means no power is reflected, while a VSWR of 2:1 represents 11% of the total power is reflected back to the transmitter.

2.2 Measurement Setup

The most common method to accurately measure the radiation efficiency of an antenna is the Gain/Directivity method which is based on anechoic chamber measurements [14]. The measurement was done at DRS's shielded anechoic chamber fitted with absorbers and RF shielding to minimize reflections. The setup includes the Antenna Under Test (AUT), a wideband log-periodic receive antenna, and turntable fitted with a 125 cm radius ground plane (Figure 3).

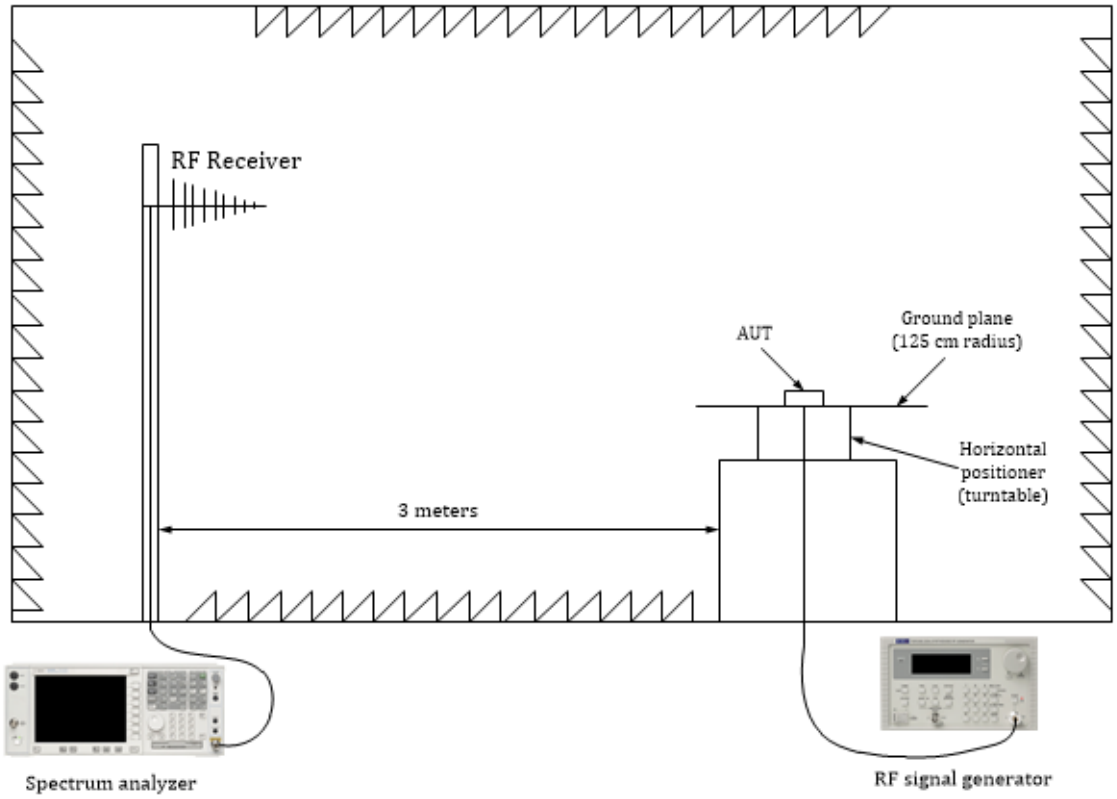

Figure 3: Measurement Setup

In this setup, the AUT is placed on top of a ground plane centred on the turntable base which rotates 360° in Azimuth. The AUT is fed with continuous wave RF signals at the UHF and VHF frequencies to transmit power. The signal is then picked up by a vertically polarized log-periodic receiving antenna with a multi element directional antenna, and the power level recorded on the spectrum analyzer. The turntable is manually rotated in azimuth and measurement data are recorded and plotted using Excel. Using the relationship between transmit power, gain of antenna and total losses in circuitry, the EIRP is calculated. The details of EIRP computation are shown in Appendix C beginning with theory of Friis transmission equation. All measured data obtained in this thesis are in far field conditions. The power fluctuation or drift in the RF signal generator is measured using a power meter and accounted for in EIRP measurements.

Chapter 3

3.0 VHF Antenna Design

Various VHF antennas were surveyed in order to meet requirements and understand the limitations of their performance. Different design alternatives were investigated to obtain the best gain, omnidirectional characteristics and linear polarization. The more typical antenna designs, such as dipole, monopole, helix, loop, patch, meandered antennas, and slots, are considered. Several other unorthodox antenna models are also explored but, will not be discussed as most were not viable solutions. Due to near field effects imposed by local obstructions where the antenna is housed, options become very limited and an intensive investigation is required to understand the behavior of electromagnetism in these environments. Variants of the traditional antennas were designed and optimized to meet requirements specified in Chapter 1; in particular, a slot antenna solution employing transmission line theory will be presented as an alternative for the transmission of 121.5 MHz antenna in the ADFR system. Some of the other antennas designed and manufactured are also presented with a brief description of their properties and electrical performance.

3.1 Slot Antenna

One of the antenna solution presented for the transmission of the 121.5 MHz signal in the ADFR beacon is the “Resonant Transmission Line” shown in Figure 4. Its operation follows the classical theory of quarter-wave transmission line, with a unique feed network discussed in Section 4.1.3. The antenna width, length and height are 12.5x2.67x1.5 inches, respectively, with its radiating elements (brown) on both sides of the cube separated by low dielectric rigid foam.

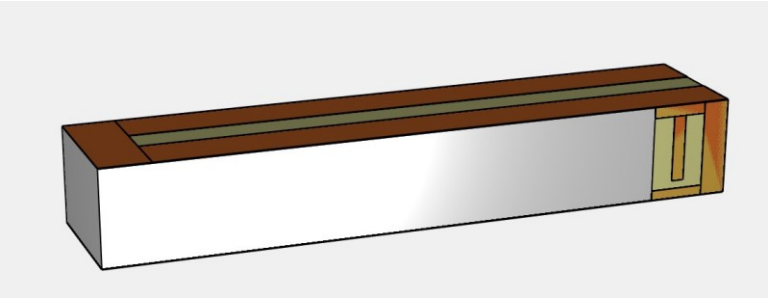

Figure 4: 121.5 MHz Antenna

The radiating elements consist of copper placed on top of an FR4 board. It can be unfolded and shown as a quarter-wave transmission line antenna, or equivalently, a slot antenna with one side of the slot open and the other side shorted (Figure 5). By reducing the length of the radiating elements, the antenna can be tuned to a frequency in the VHF range.

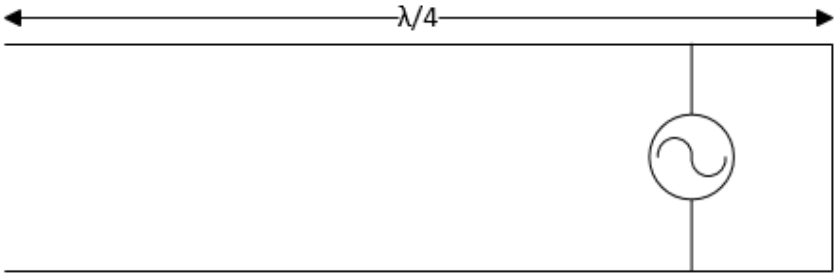

Figure 5: 121.5 MHz equivalent quarter-wave slot antenna with one side open and other side shorted

The antenna is fed with a coax cable as shown in Figure 6. It is built on a dielectric material of 4 ($\epsilon = 4$) and fed on the short-ended side of the transmission line in such a way 50 Ω impedance match is achieved at 121.5 MHz. The theory of operation follows that of a resonant transmission line tapped for impedance matching. For a better understanding of how transmission lines work, the quarter-wave transformer is described first using the transmission line theory for lossless and lossy lines, and later we will explore the quarter-wave tapped resonant line and how it is closely related to the half-wave slot antenna.

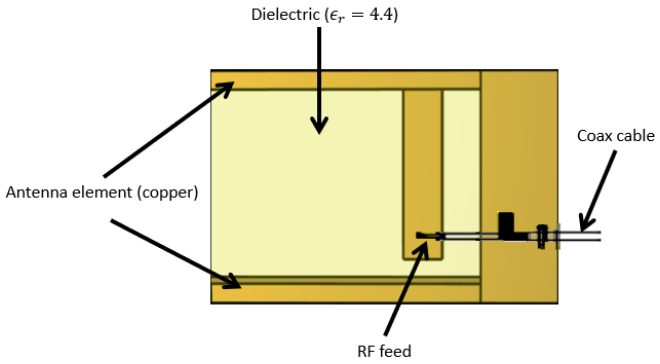

Figure 6: 121.5 MHz antenna Feed Network

3.1.1 Theory

Quarter-wave Transformer

A quarter-wave ($\lambda/4$) transformer (Figure 7) is a simple impedance transformer used in matching real load impedance to a transmission line to minimize the power reflected from the load to the source down the transmission line. It has the useful property of transforming impedance into its reciprocal with respect to the characteristic impedance of the line.

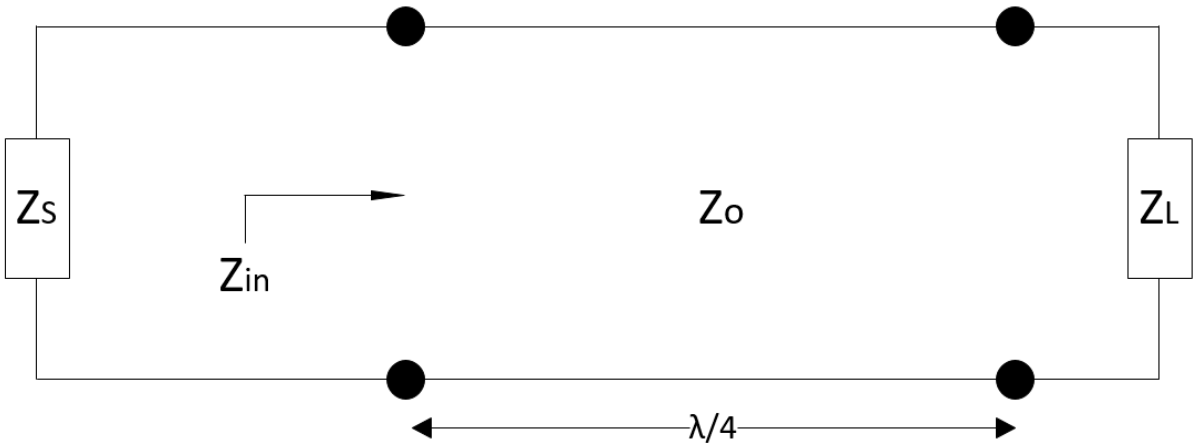

Figure 7: Transmission Line with quarter-wave section

To have a matching condition, the input impedance (Z_{in}) should be equal to the impedance of the source (Z_s).

Assuming a lossless line, the propagation constant, γ, is given in [15] as,

$$\gamma = \alpha + j\beta = \sqrt{(R + j\omega L)(G + j\omega C)} \tag{13}$$

Since the series resistance per unit length, R, and conductance per unit length, G, are assumed to be negligible (i.e. $R = G = 0$), the real component $\alpha \approx 0$ while the γ term reduces to,

$$\gamma = j\omega\sqrt{LC} \tag{14}$$

The phase constant β is therefore,

$$\beta = \omega\sqrt{LC} \tag{15}$$

From transmission line theory, the input impedance of a section of a lossless line is given in [15]:

$$Z_{in} = Z_o\left(\frac{Z_L + jZ_o \tan\beta l}{Z_o + jZ_L \tan\beta l}\right) \tag{16}$$

where Z_{in} is the input impedance, Z_L is the load impedance, Z_o is the characteristic impedance of the $\frac{\lambda}{4}$ transformer, β is the phase constant per unit length given as $\beta = \frac{2\pi}{\lambda}$, and l is the length of the transformer. Since,

$$\beta l = \frac{2\pi}{\lambda} \times \frac{\lambda}{4} = \frac{\pi}{2} \quad \Longrightarrow \quad \tan\beta l = \tan\frac{\pi}{2} = \infty$$

If the length of the transmission line is $l = \frac{\lambda}{4}$, then the input impedance looking towards the load is:

$$Z_{in} = \frac{Z_o^2}{Z_L} \tag{17}$$

For a lossy line, the effect of the series resistance (R) and dielectric conductance (G) are included. By rearranging the γ expression and using the binomial expansion,

$$\gamma = \alpha + j\beta = \sqrt{(R + j\omega L)(G + j\omega C)} = \sqrt{\left(\frac{G}{j\omega C} + 1\right)\left(\frac{R}{j\omega L} + 1\right)(j\omega C)(j\omega L)}$$
$$= j\omega\sqrt{LC}\sqrt{1 - \left(j\left(\frac{G}{\omega C} + \frac{R}{\omega L}\right) - \frac{RG}{\omega^2 LC}\right)} \tag{18}$$

For a low loss transmission line, the limits for the conductance (G), resistance (R), inductance (L) and capacitance (C) per unit length are,

$$\omega C \gg G \qquad \omega L \gg R \qquad \Longrightarrow \qquad \omega^2 LC \gg GR$$

$$\gamma \cong j\omega\sqrt{LC}\left(1 - \frac{j}{2}\left(\frac{G}{\omega C} + \frac{R}{\omega L}\right)\right) = \frac{1}{2}\left(R\sqrt{\frac{C}{L}} + G\sqrt{\frac{L}{C}}\right) + j\omega\sqrt{LC} \tag{19}$$

The attenuation factor, α, can be approximated as,

$$\alpha \cong \frac{1}{2}\left(R\sqrt{\frac{C}{L}} + G\sqrt{\frac{L}{C}}\right) = \frac{1}{2}\left(\frac{R}{Z_o} + GZ_o\right) \tag{20}$$

For a lossy line where $\alpha \neq 0$, the input impedance of the transmission line is given as:

$$Z_{in} = Z_o\left(\frac{Z_L + jZ_o \tanh \gamma l}{Z_o + jZ_L \tanh \gamma l}\right) \tag{21}$$

This principle can be applied to match an antenna to a transmission line-feed. Generally, we want the impedance of an antenna which is purely resistive to match the characteristic impedance of the source line. This is done by inserting a quarter-wavelength line section with characteristic impedance (Zo).

Input Impedance of Tuned Transmission Line

A resonant line is resonant at one specific frequency. It may act either as a parallel resonant or as a series resonant. This is done by short circuiting the transmission line at the output end and cutting it to some multiple of a quarter-wavelength as in Figure 8. A parallel resonance circuit behaves as a short-circuited section of a line at odd multiples of $\frac{\lambda}{4}$; similarly, a series resonance circuit is equivalent to an open circuit at even multiples of $\frac{\lambda}{4}$.

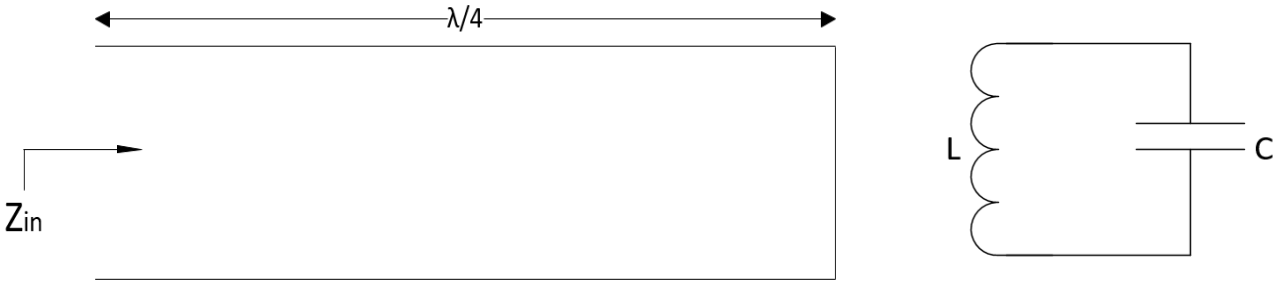

Figure 8: Tuned quarter-wave transmission line (left) and its equivalent circuit (right)

For a lossy line, the impedance of a short-circuited line of Figure 8 is given as,

$$Z_{in} = Z_o \tanh \gamma l = Z_o \left(\frac{\sinh \alpha l \cos \beta l + j \cosh \alpha l \sin \beta l}{\cosh \alpha l \cos \beta l + j \sinh \alpha l \sin \beta l} \right) \quad (22)$$

For line lengths that are an odd multiple of a quarter-wavelength, $\sin \beta l = \pm 1$ and $\cos \beta l = 0$. For a quarter-wave line, the input impedance becomes,

$$Z_{in} = Z_o \frac{\cosh \alpha l}{\sinh \alpha l} \quad (23)$$

Assuming $\alpha l \approx 0$, as is generally true for sections of low loss line, $\cosh \alpha l \approx 1$ and $\sin \alpha l \approx \alpha l$ so that,

$$Z_{in} = \frac{Z_o}{\alpha l} \quad (24)$$

For a lossy line, α was earlier approximated to be,

$$\alpha = \frac{1}{2} \left(\frac{R}{Z_o} + G Z_o \right) \quad (25)$$

For air dielectric lines, the losses due to the conductance, G, are negligible [15], therefore G can be neglected and,

$$\alpha = \frac{1}{2} \left(\frac{R}{Z_o} \right) \quad (26)$$

Substituting this α expression into Z_{in} gives,

$$Z_{in} = \frac{Z_o}{\alpha l} = \frac{2Z_o^2}{Rl} \tag{27}$$

When the quarter wave section shorted at one end is tapped at some point x along its length (Figure 9), a correspondence between this circuit and the simple low-frequency parallel or series resonant circuit is observed.

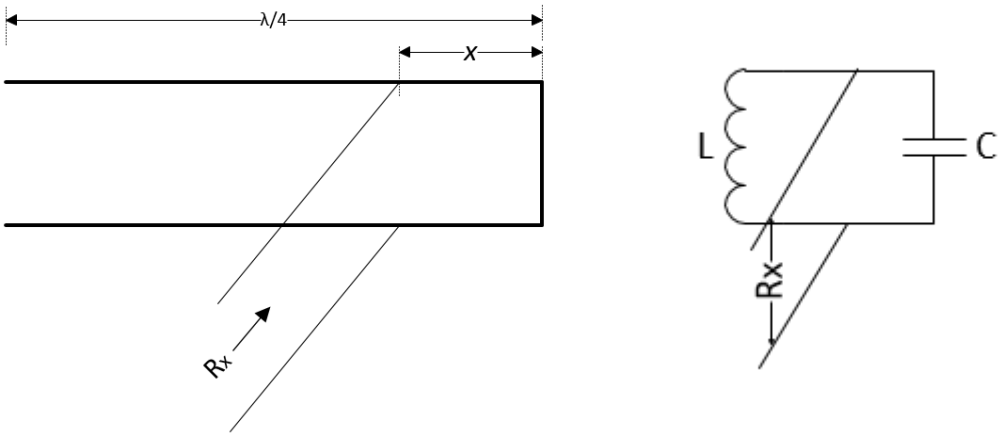

Figure 9: Tapped quarter-wave transmission line (left) and its equivalent circuit (right)

The reactance looking toward the shorted end will be inductive with a value,

Lossless lines: $$Z_{SC} = jZ_o \tan \beta x \tag{28}$$

Lossy lines: $$Z_{SC} = jZ_o \tanh \gamma x \tag{29}$$

The reactance looking toward the open end will be capacitive, equal in magnitude but opposite in sign. This is given by:

Lossless lines: $$Z_{OC} = jZ_o \tan\beta\left(\frac{\lambda}{4} - x\right) = -jZ_o \tan\beta x \quad (30)$$

Lossy lines: $$Z_{OC} = jZ_o \tanh\gamma\left(\frac{\lambda}{4} - x\right) = -jZ_o \tanh\gamma x \quad (31)$$

The equal but opposite reactance are in parallel just as shown in Figure 9 (right), and the input impedance will be purely resistive. The impedance seen at location $l = x$ when the tap point is moved from shorted end toward the opened end is a pure resistance that varies from zero to a high impedance value. Typically, these lines are relatively high Q and considered to have a sinusoidal voltage distribution along the line [15] making it easy to understand how the input resistance varies as the tap point (x) is moved along the quarter-wave section. When current flows through the line, some energy is dissipated in the form of heat (or I^2R loss). The input power supplying the losses is equal to

$$P_{in} = \frac{V^2{}_{in}}{R_{in}} = \frac{V^2{}_{in}\, Rl}{2Z_o^2} \quad (32)$$

where V_{in} is the voltage at the open end of the section, and R_{in} is the input resistance at the open end of the section.

When the tap point of the feed line is at a distance x from the shorted end (Figure 9), the power input is given by

$$P_{in} = \frac{V^2{}_x}{R_x} \quad (33)$$

where R_x is the input resistance at the point x, and V_x is the voltage at this point with a sinusoidal voltage of $V_x = V_{in} \sin\beta x$. The input power at any point x is therefore given by

$$P_{in} = \frac{V^2{}_x}{R_x} = \frac{V_{in}^2 \sin^2 \beta x}{2Z_o^2} = \frac{V_{in}^2 \, Rl}{2Z_o^2} \tag{34}$$

Thus, the input resistance varies as the square of the sine of the angular distance from the shorted end or:

$$R_x = \frac{2Z_o^2}{Rl} \sin^2 \beta x \tag{35}$$

To analyze the antenna in Figure 4, the circuit in Figure 10 is shown to illustrate the equivalence to a transmission line.

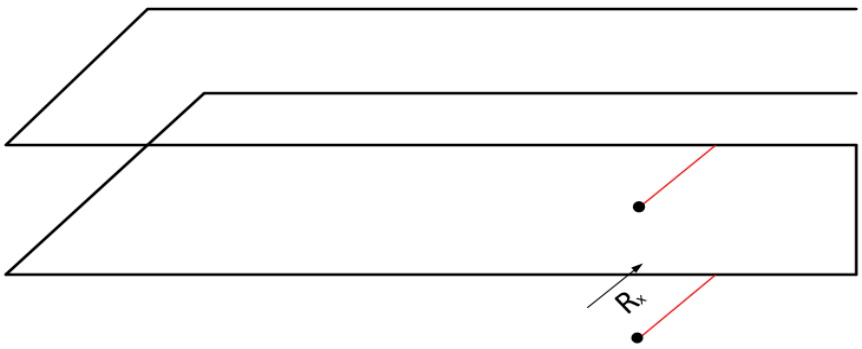

Figure 10: Simplified drawing of Figure 4

From Figure 10, it is easy to realize this is a transmission line with a short on one end and open on the other with both conductors of the transmission line measuring $\frac{\lambda}{4}$ each. Assuming the characteristic impedance of the quarter-wavelength line is lossless, the input impedance can be evaluated using transmission line theory.

The problem can be broken and analyzed in two parts, a resonant transmission line antenna and a slot antenna.

Slot Antennas

To understand the antenna in Figure 10, we further need to introduce the concept of slot antennas. Slot antennas were developed to solve design issues arising from requiring antennas that do not protrude from a flat surface on which they reside, such as the skin of an aircraft. They are simple cut outs from conductive sheet and when fed by a generator or transmission line, it radiates EM waves with a pattern like that of a dipole.

The slot antenna can be thought of as a pair of transmission lines consisting of parallel conducting planes separated by distance, *h* (Figure 11). The conductor is bonded to the metal sheet as shown in Figure 12.

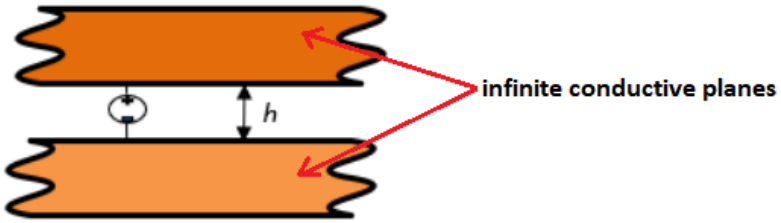

Figure 11: Infinite planes acting as a transmission line excited by a voltage source

Such a transmission line could be excited by a current or voltage source by means of a coaxial cable whose shield and center conductor are connected to each conducting plane. The voltage across the two planes would be that of an infinite transmission line while the electric field propagation would be directed towards the slot openings. If the open ends of the transmission planes are short circuited at both ends, a standing wave would be setup and the electric field and voltage distribution would be that of a lossy short-circuited transmission line. This is effectively a rectangular slot antenna looking like Figure 12.

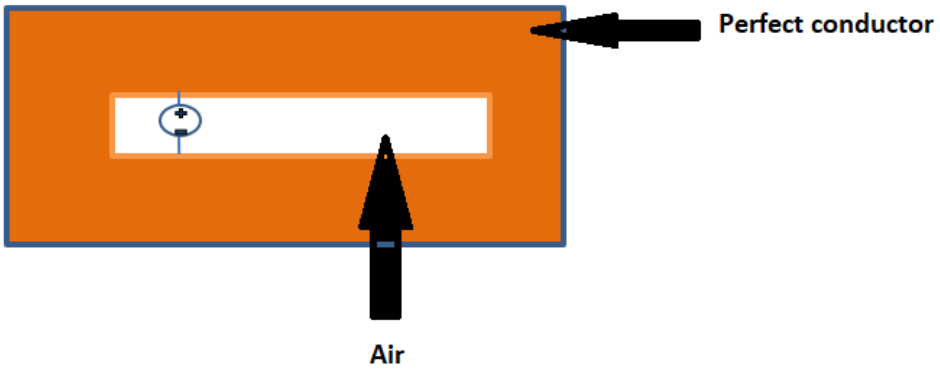

Figure 12: Slot antenna

To analyze the slot antenna further, we look at the slot filled with air connected to a voltage source as shown in Figure 13. For this analysis, assume $h << \lambda$ and the length of the slot, L, to be $\frac{\lambda}{2}$.

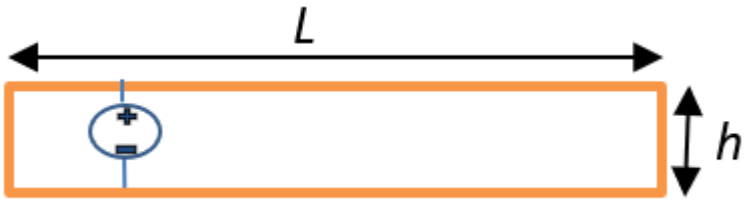

Figure 13: Slot with voltage source

The voltage at the short ends of the slot is zero while the peak is at the center. The current distribution along the line can be obtained by splitting the slot into two shorted transmission lines. From general transmission line theory, we know for short circuited transmission lines, the standing wave voltage and current profiles are offset with respect to each other as illustrated in Figure 14. Therefore, the current is a maximum at the shorted ends and minimum and the center.

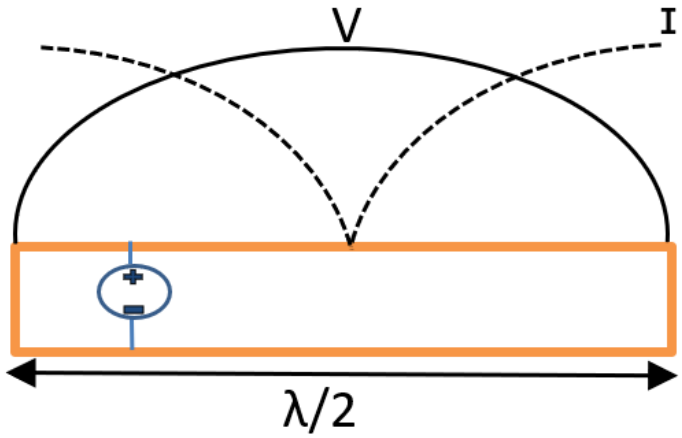

Figure 14: Voltage and current distribution along a line

The radiation of a slot antenna is due to the voltage distribution along the slot. The associated electric field is directed across the slot which gives rise to radiation. Notice in Figure 14, at the center of the slot, the current is minimum, and voltage is maximum which means the impedance goes to infinity ($Z = V/I = \infty$). If the slot was fed right at the short ends, the result would be a very low impedance according to $Z = V/I$. Therefore, the location of the feed is moved along the slot until the antenna is matched to a desired impedance (typically 50Ω). This is done since the reactive components cancel each other out, leaving pure resistance.

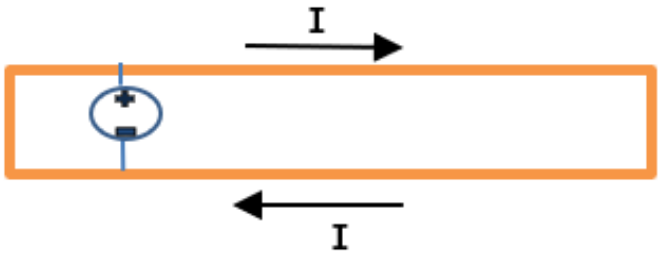

Figure 15: Current flow along a slot antenna

Consider the half-wavelength slot antenna in Figure 14. If the feed was moved closer to the edge, as in Figure 15, we can break the slot into two shorted transmission lines: a transmission line < $\lambda/4$ and a transmission line > $\lambda/4$ (Figure 16).

Figure 16: Transmission line < $\lambda/4$ (left) and Transmission line > $\lambda/4$

The impedance of a transmission line length < $\lambda/4$ and > $\lambda/4$ is given in [16] as:

$$Z_{SC} = jZ_o \tan \beta l \tag{36}$$

More importantly, for a line length less than a quarter wavelengths the shorted section is equivalent to an inductance, while a line with a length greater than a quarter wavelengths the shorted section is equivalent to a capacitance. If we replace the lines in Figure 16 with their equivalents, we end up with Figure 17, where L, C, and R are inductance, capacitance and resistance, respectively. The radiation resistance for a lossy line was earlier determined to be

$$R_x = \frac{2Z_o^2}{Rl} \sin^2 \beta x \tag{37}$$

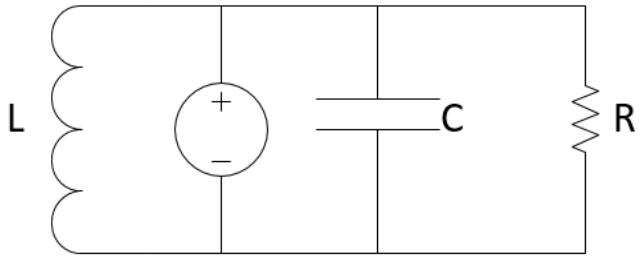

Figure 17: Equivalent circuit of resonant slot antenna

For a properly tuned antenna, the reactive components L and C would cancel out and all that is left is the radiation resistance R. When R is matched to the source impedance, the maximum power will flow into the antenna. Note, the half-wave slot is equivalent to a quarter-wave slot with an open circuit.

Radiation Pattern

The radiation pattern of a slot antenna is often described by its 'dual' antenna (Figure 18). The concept of duality relates the radiated fields and impedance of a slot antenna to that of the field of its dual antenna, the dipole.

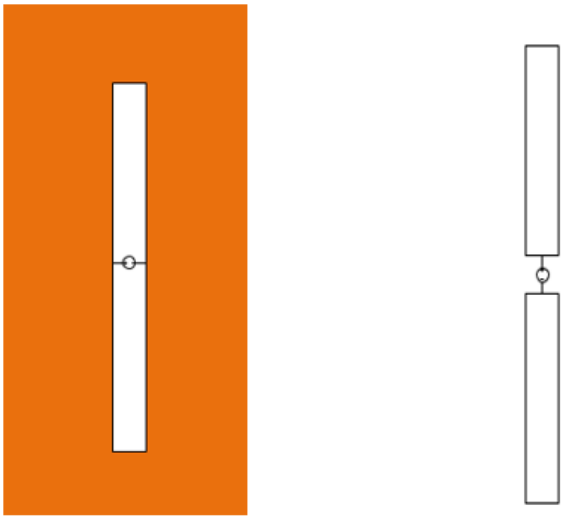

Figure 18: Dual antennas: (left) Slot antenna (right) dipole antenna

If we consider a slot in a conducting plane (left) with a feed point at the center, the electric field would be that of a shorted transmission line with a standing wave setup. The slot antenna is similar to the dipole antenna where the feed occurs at the center of the dipole.

According to Babinet's principle, the impedance of the slot (Z_s) and dipole antennas (Z_d) (the duals) are related by:

$$Z_s Z_d = \frac{\mu}{4\epsilon} \tag{38}$$

where,

$\mu = 4\pi \times 10^{-7}$ $\left[\frac{H}{m}\right]$ is the magnetic permeability

$\epsilon = 8.854 \times 10^{-12}$ $\left[\frac{F}{m}\right]$ is the permittivity of free space

Equivalently, we can write the above equation in the general form by replacing it with the free-space characteristic impedance (η),

$$Z_s Z_d = \frac{\eta^2}{2} \tag{39}$$

$$\eta = \sqrt{\frac{\mu}{\epsilon}} = 377\ \Omega \tag{40}$$

The above equation is powerful in that it may now be employed to find the impedance of a slot antenna, given the impedance of the complementary dipole antenna. Since the input impedance of a theoretical half-wave dipole is $Z_d = 73 + j43$, the impedance of the theoretical half-wave slot antenna would then be,

$$Z_s = \frac{377^2}{4 \times (73 + j43)} = 361 - j213$$

Note the impedance of the slot antenna is much larger and capacitive, while the impedance of the dipole antenna is smaller and inductive.

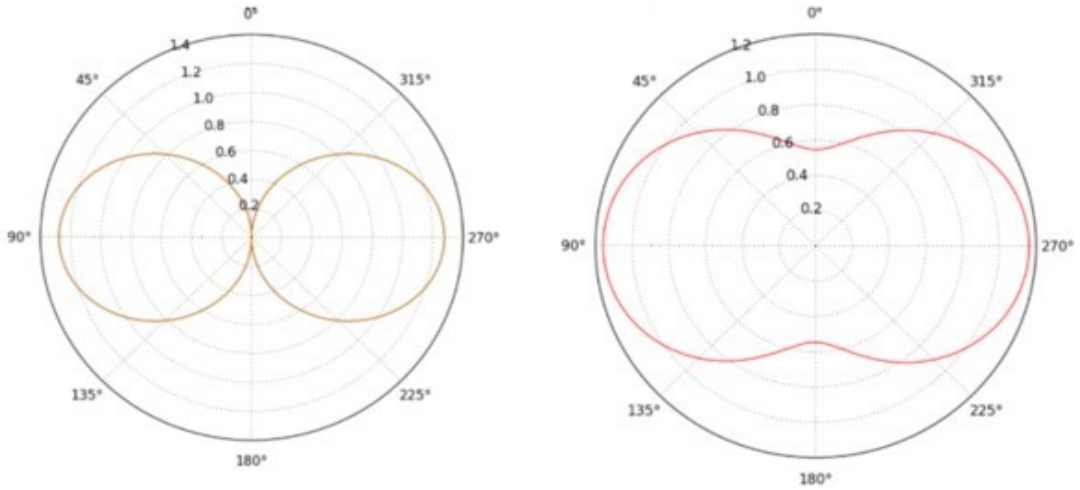

Figure 19: Radiation pattern of dipole (left) and ADFR 121.5 MHz antenna (right)

It is stated in [16] that the radiation pattern of a narrow slot antenna is the same as that of its dual antenna (dipole), with the exception the electric and magnetic fields are interchanged. As a result, the polarization is rotated, so that radiation from vertical slot is polarized horizontally. This makes it easy to estimate field properties of a narrow slot antenna from a dipole antenna whose solution is already known. Furthermore, the $\frac{\lambda}{2}$ slot antenna is equivalent to a $\frac{\lambda}{4}$ slot antenna with an open circuit, with Figure 19 showing the similarity between radiation patterns of an ideal dipole versus the 121.5 MHz antenna designed in Figure 4.

3.1.2 Antenna Test and Evaluation

Simulation

The primary tool used to simulate is EMPIRE XPU. As time domain simulator, it is effective in simulating a range of frequencies instead of a single one as in frequency domain simulators while allowing to do full wave 3D simulations.

The slot antenna in Figure 4 was simulated and the results compared against the performance of a $\frac{\lambda}{4}$ vertically polarized reference monopole over a $\frac{\lambda}{2} = 1.25\,m$ radius ground plane. The radiation pattern in free space of this antenna is similar to that of an isotropic radiator. The ground plane plays a big role in the radiation pattern for any antenna in the near field. To model a real-life application, a ground was chosen 1 inch (2.54 cm) below the antenna element oriented as shown in Figure 20.

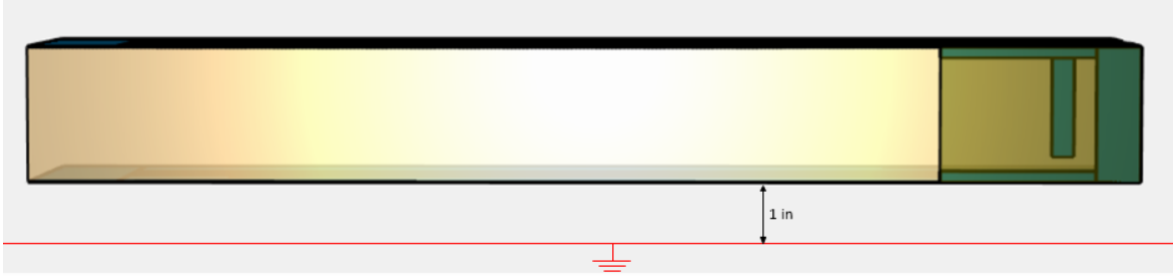

Figure 20: Orientation of slot antenna with respect to ground

The simulated results are shown in Figure 21. The reduced field intensity at the feed end was expected due to the feed's proximity to ground. Furthermore, by observing Figure 22 it can be noticed the shift in field intensity is more at the feed end where the standing waves initially develops as illustrated on the left of Figure 23. Also shown is the direction of current flow (left) and electric field view (right) where the standing wave forms.

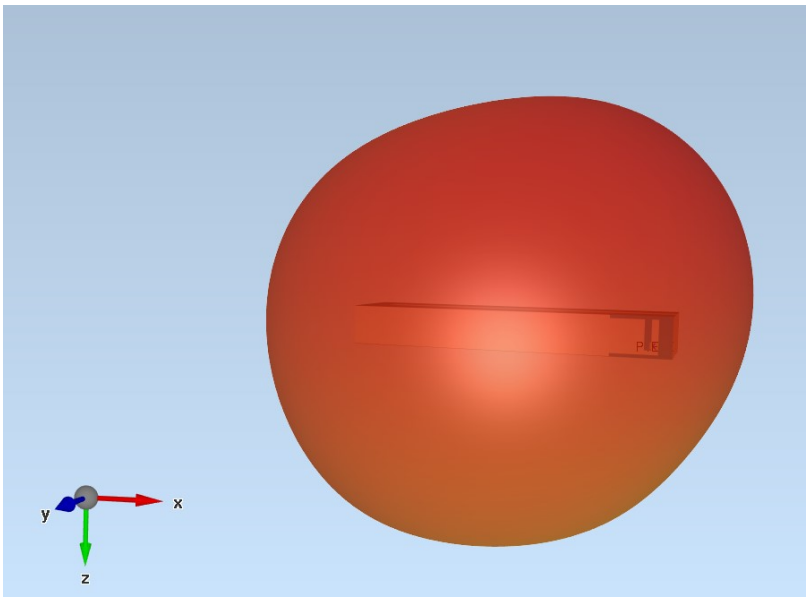

Figure 21: Simulated radiation pattern of slot antenna in Figure 4

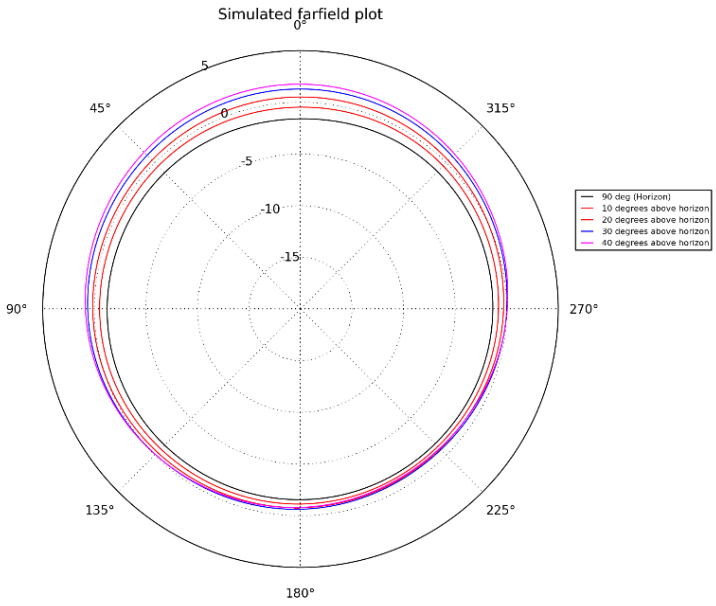

Figure 22: 2D far-field pattern in different elevation cuts

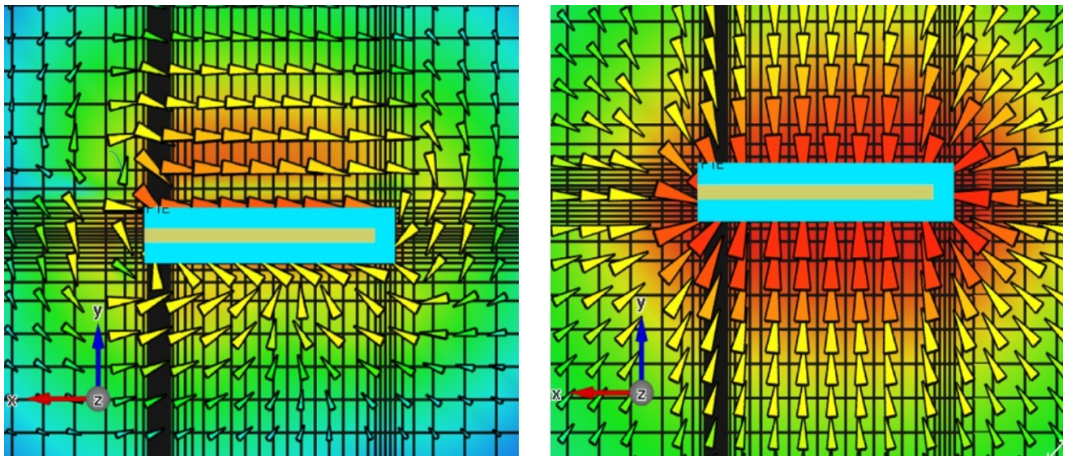

Figure 23: Surface current density (left) and E-field view of antenna in Figure 5.4 (right)

Note, Figure 24 shows the orientation of the antenna with respect to ground plane. The maximum directivity obtained from the simulation was 1.5 dBi.

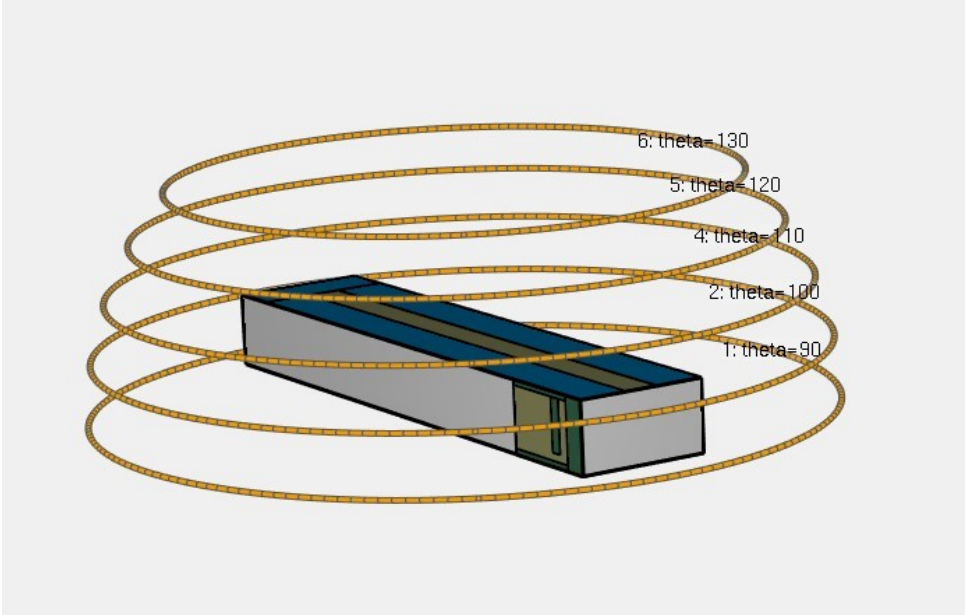

Figure 24: Antenna orientation with respect to elevation angle

Measured Results

The slot antenna and reference monopole were tested and measured under the same condition in an anechoic chamber. Radiation patterns in two elevation cuts were recorded and are presented in Figure 25 for a 10° elevation and Figure 26 for 20° elevation.

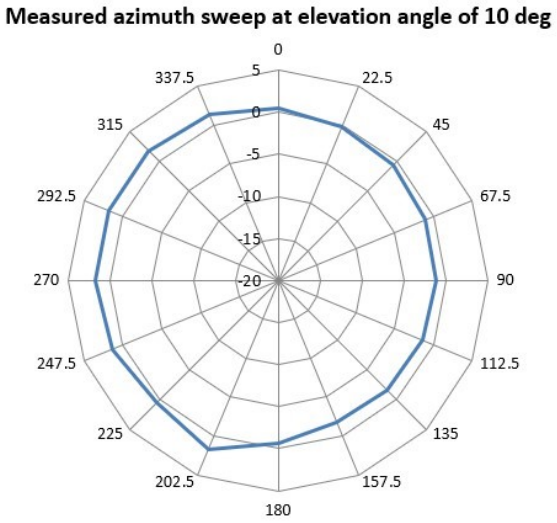

Figure 25: Measured pattern at 10 degrees elevation

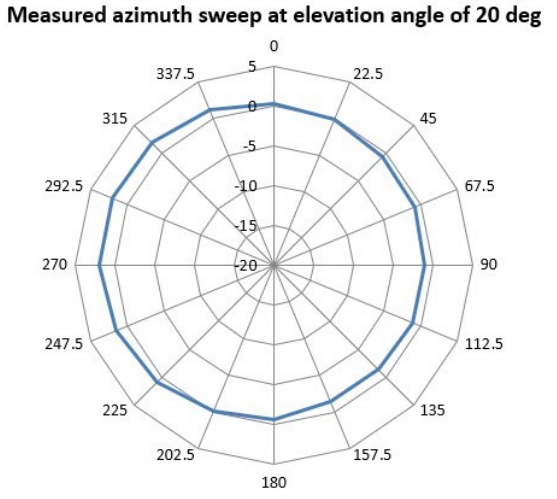

Figure 26: Measured pattern at 20 degrees elevation

The maximum measured directivity was 2.1 dBi at 20° elevation while the minimum recorded directivity was -1.8 dBi at the 10° elevation cut. The results are almost identical to the simulations, although in some azimuth angles the AUT has lower gain compared to the simulation, while on other angles the response is better. This is related to the installation of the AUT on the metal ground plane, and hence is not centred in the receiver antenna's line of sight. The measured results are comparable to simulation results with negligible difference. The pattern follows that of a typical slot antenna with most of the fields concentrated at higher elevation angles.

3.1.3 Antenna Sensitivity Analysis

The feed point of Figure 6 is critical in matching the antenna impedance to 50 Ω. By moving the feed from the shorted end towards the open end as indicated in Figure 27, the radiation impedance can be matched to 50 Ω while eliminating the reactive components. In order to identify the optimum feed location, a sensitivity analysis was performed to understand the capacitive and inductive effects on the matching network. The feed stub was swept in the horizontal (Figure 27) and vertical (Figure 33) planes and the effect was analysed.

Horizontal Sweep View

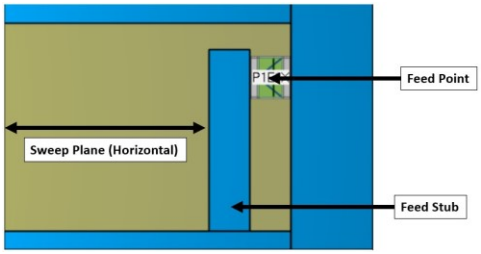

Figure 27: Antenna Feed Network (Horizontal)

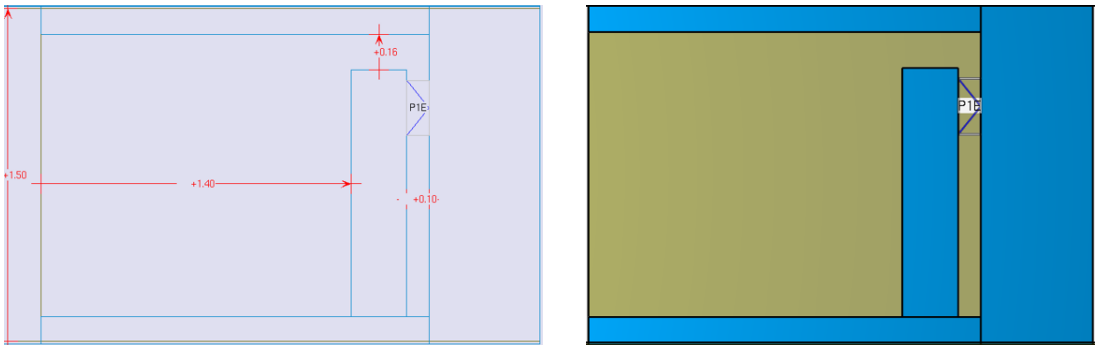

Figure 28: Stub spaced 0.1 inch horizontally

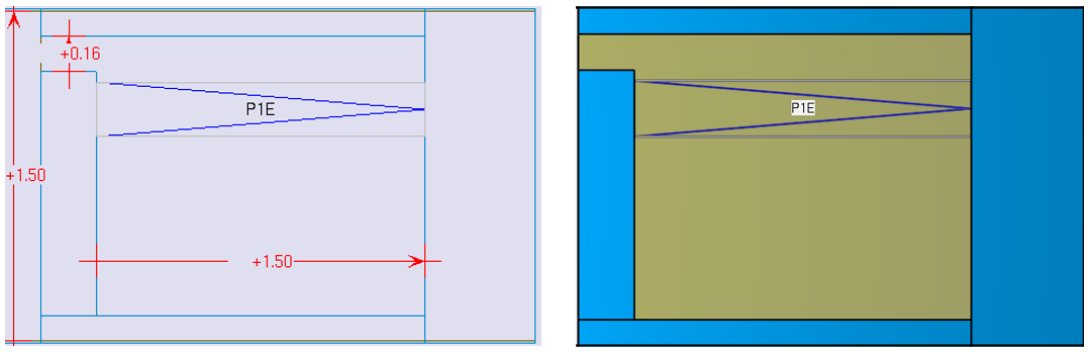

Figure 29: Stub spaced 1.5 inch horizontally

Return Loss (S11) - Horizontal Sweep

As the stub's space increases horizontally from Figure 28 to Figure 29, the center frequency increases while the return loss (S11) gets worse. The closer the stub is to the feed point the better it performs. Figure 30 shows a 0.1 inch spacing gives the best performance.

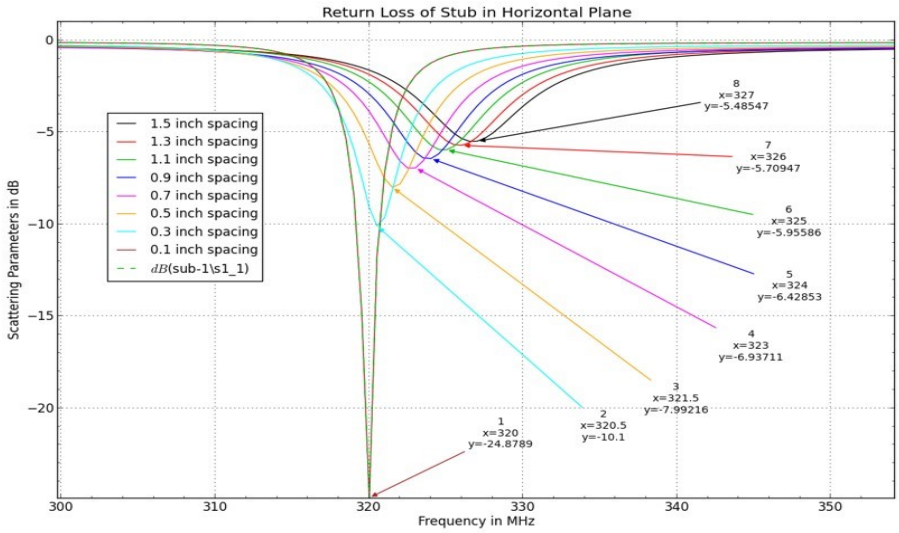

Figure 30: Horizontal Sweep (S11)

Impedance - Horizontal Sweep

Figure 31 and Figure 32 show the resistive and reactive sweeps. As the spacing of the stub increases, the real component of the impedance decreases. The closer the stub is to the feed point the better it is matched to 50 Ω.

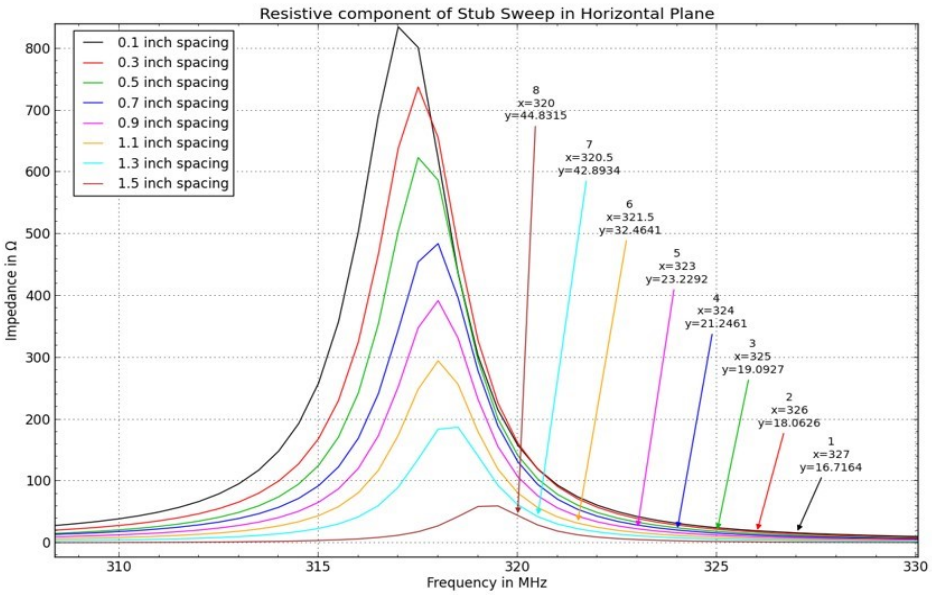

Figure 31: Impedance for Horizontal Sweep (Resistance)

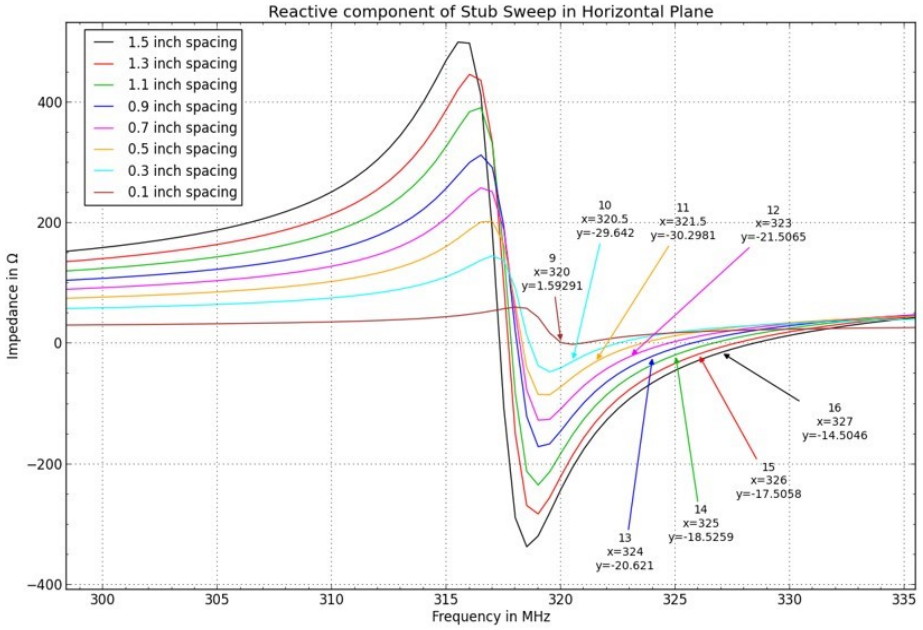

Figure 32: Impedance for Horizontal Sweep (Reactance)

The reactive component is mostly capacitive and does not follow a generic trend. At 0.1 inch spacing the lowest reactance is shown indicating a close match. However, as the stub spacing increases it appears the capacitance decreases which is an expected behaviour.

Table 3: Resistive and reactive component of horizontal stub sweep

Horizontal Spacing [inch]	Resistive (Ω)	Reactive (Ω)	S11 [dB]
1.5	44.8	-14.5	-5.5
1.3	42.9	-17.5	-5.7
1.1	32.5	-18.5	-6.0
0.9	23.2	-20.6	-6.4
0.7	21.2	-21.5	-7.0
0.5	19.1	-30.3	-8.0
0.3	18.1	-29.6	-10.1
0.1	16.7	1.6	-24.9

Vertical Sweep View

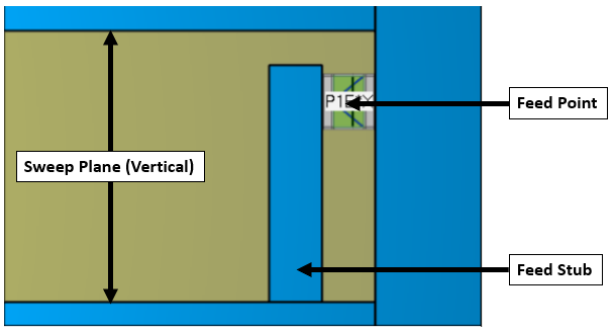

Figure 33: Antenna Feed Network (Vertical)

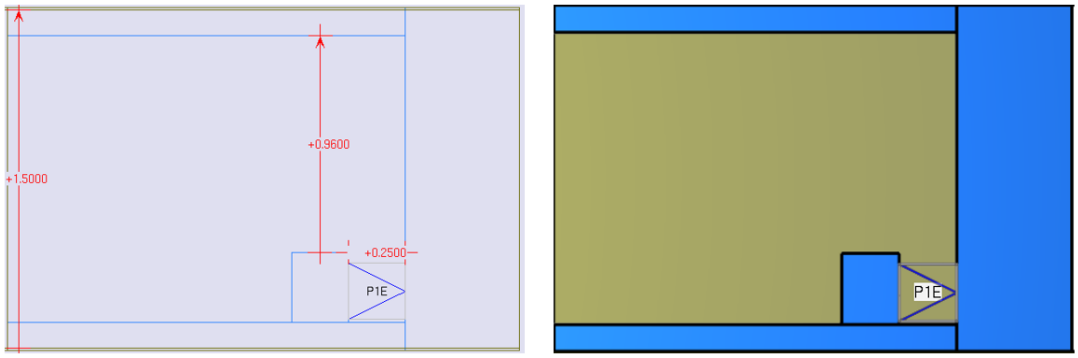

Figure 34: Stub spaced 0.96 inch vertically

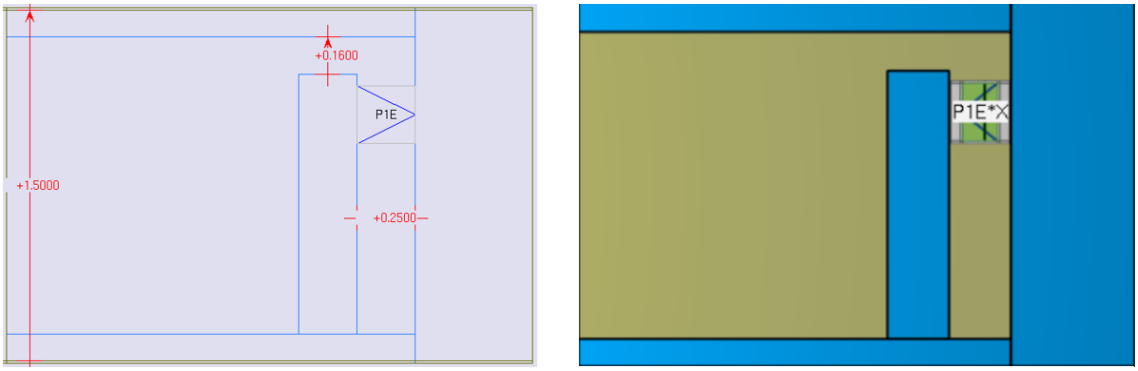

Figure 35: Stub spaced 0.16 inch vertically

Return Loss (S11) - Vertical Sweep

Figure 36 shows the height of the stub when is swept vertically, the return loss response at spacings 0.96 inch, 0.76 inch and 0.56 inch are good. We look at the impedance to verify whether a good match is also present at these resonant frequencies.

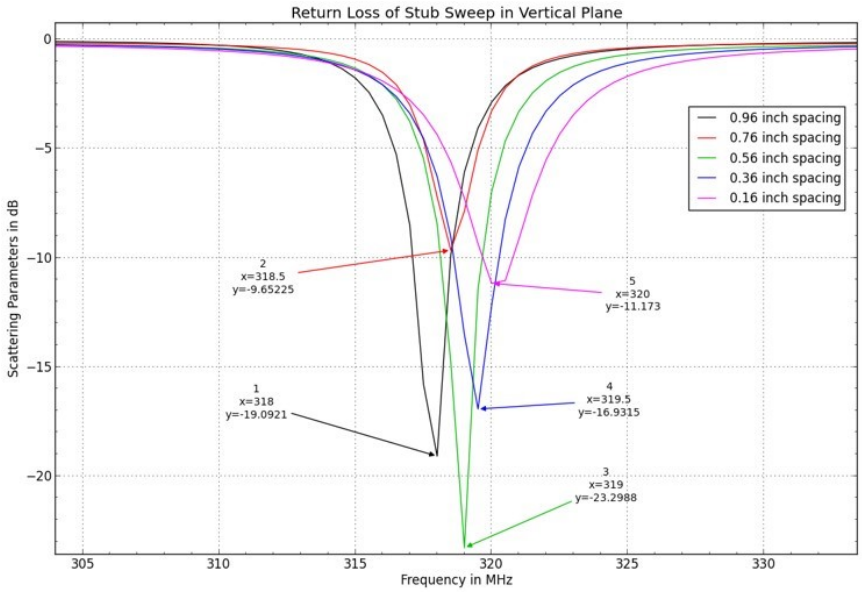

Figure 36: Vertical Sweep (S11)

Impedance - Vertical Sweep

From Figure 36, we observed strong return loss at spacing 0.96 inch, 0.76 inch and 0.56 inch, however, Figure 37 shows only 0.96 and 0.76 inch spacing resulted in close to 50 Ω impedance. At 0.36 inch and 0.16 inch spacings, the impedance was very close to 50 Ω however it is likely that there is a higher reactance in these frequencies of interest.

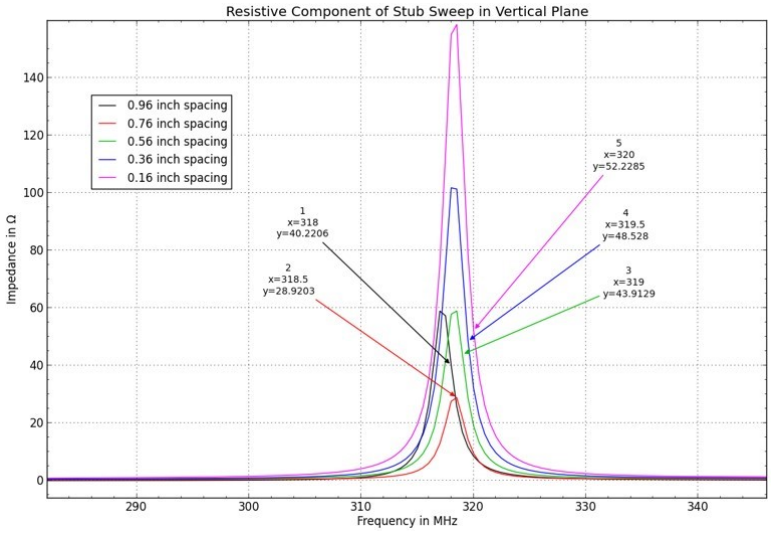

Figure 37: Stub spaced 0.16 inch vertically

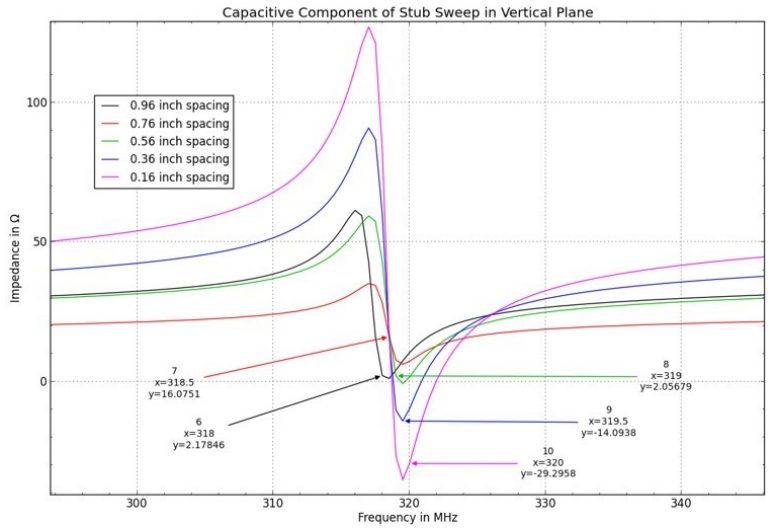

Figure 38: Impedance for Horizontal Sweep (Reactance)

The result shows inductive behaviour at smaller spacings but capacitive behaviour as the spacing in the vertical plane increases. As noted earlier, although the resistive component was closer to 50 Ω, that came at a cost of higher reactance which is undesirable. The reactance remained low and capacitive at higher spacing particularly at 0.96 and 0.56 inch spacing.

Table 4: Resistive and reactive component of vertical stub sweep

Vertical Spacing [inch]	Resistive (Ω)	Reactive (Ω)	S11 [dB]
0.96	40.2	2.2	-19.1
0.76	28.9	16	-9.6
0.56	43.9	2.1	-23.3
0.36	48.5	-14.1	-16.9
0.16	52.2	-29.3	-11.2

3.2 Alternative VHF Antennas

3.2.1 Spiral Slot Antenna

Radiation pattern measurement was performed using a 'Spiral-slot' antenna coiled in a high-density foam material, Figure 39. Testing and measurement was performed in an anechoic chamber including the antenna sensitivity to near field objects. Different sizes were modelled and fabricated of which the best possible antenna with EIRP values high enough to exceed ED-62A requirements. A few aspects of the wrapped slot antenna performance are listed below.

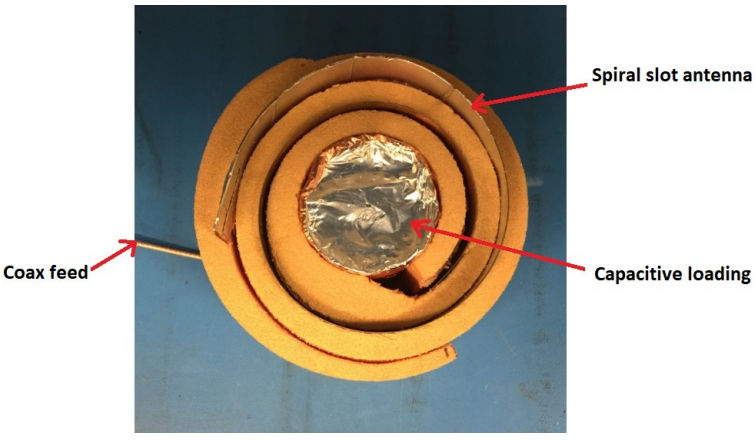

Figure 39: Spiral-slot antenna

- Vertical polarization was achieved as per ED-62A.
- The antenna performed reasonably well with an average EIRP of 60 mW in azimuth, which is 10mW more than the current minimum requirement with a VSWR 3.5:1.
- A very narrow bandwidth of 1 MHz was achieved which is inherently not good for emergency beacons that might be subjected to water immersion. Antennas tend to easily detune in water and especially those antennas with narrow bandwidth.
- Mutual coupling with neighbouring transmitting antennas was an issue for this slot antenna. Although solutions and techniques exist to prevent antennas from interfering with each other, it was not the scope of this research.
- This antenna was subjected to extreme temperature testing to study the effect of hot temperature and cold temperatures had on the performance. Minimal change was exhibited by this antenna which was an important attribute in ELT beacons.

3.2.2 Meandered Dipole Antenna

The meandered dipole antenna concept in Figure 40 was designed and simulated and showed poor performance in the azimuth plane. Also, the radiation pattern was not omnidirectional as per ED-62A requirements. On the other hand, the polarization was vertical with a narrow bandwidth of about 2 MHz. It was expected to be lossy like any other wire antennas, but most importantly the effect on nearby antenna radiation pattern is significant.

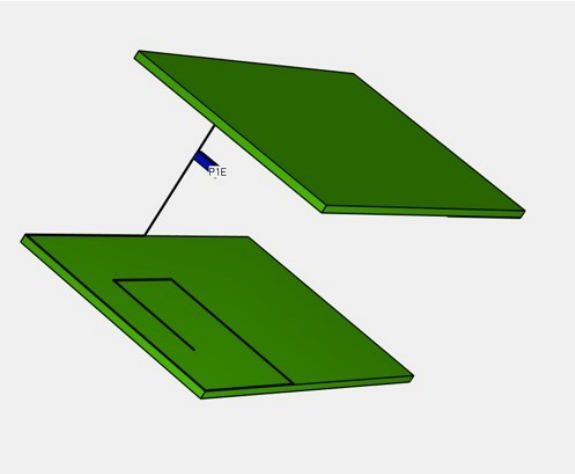

Figure 40: Meandered dipole antenna

3.2.3 Vivaldi-on-Cylinder Antenna

A Vivaldi-type antenna was modelled on a cylinder with a high dielectric constant (Figure 41). The idea was to take a planar antenna which operates over a wide frequency range and mount it on a non-planar substrate while maintaining its remaining properties.

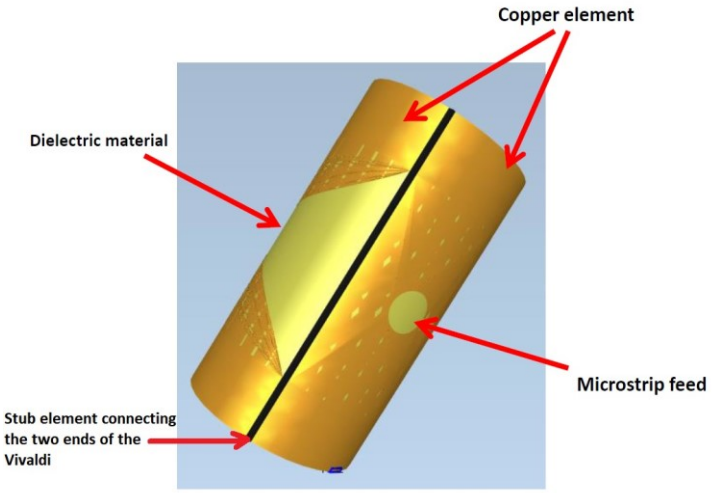

Figure 41: Vivaldi conformed on a cylinder

The results are inconclusive; however, early simulation show promising results. A python script included in Appendix D was written to simulate the antenna on EMPIRE XPU. It is expected to demonstrate a wideband property due to the nature of its geometry. Since the Vivaldi is a directive antenna, wrapping it along a cylinder so that the two ends are electrically connected will produce an omnidirectional pattern along the cylinder.

3.3 Chapter Summary

A survey of antennas in the VHF band was explored and revealed the challenges faced by the industry to meet strict requirements and survive under the harshest conditions. The main challenge of designing VHF antennas for deployable ELTs is packaging, because the size of the antennas is small compared to its wavelength. In particular, the wavelength of VHF antennas is in the order of 2 meters, therefore a simple packaging solution is not an easy task to achieve, especially in case of the ADFR, the antenna unit is exposed to near field effects from surrounding components interacting and interfering with transmitted signals which result in poor antenna performance. A highly performing antenna can certainly be designed to operate in free space, but ultimately its performance should be judged in the environment where it will be used. For that reason, when designing a good performing antenna, parameters such as near field effect must be considered beforehand so that design margin may be applied.

Several antennas with different shapes and sizes were reviewed while keeping in mind the minimum requirements set for the operation of the 121.5 MHz antenna. Their properties were studied by first simulation and then fabricating units that showed to have higher potential. Most were considered not to be the best suited solution for the ADFR due to either their electrical performance or physical size.

The proposed folded slot antenna showed the most promising performance with good omnidirectional characteristics at 121.5 MHz with a measured gain of 2.1 dBi and -1.8 dBi at 20° and 10° elevation angles, respectively. The simulated directivity was 1.5 dBi at elevation angles above 20°. Simulation also showed for elevation angles less than 60°, the radiation pattern maintains omnidirectionality within 3 dB. Parametric studies were carried out to optimize the feed network and match the impedance of the slot antenna to 50 Ω while maintaining sufficient bandwidth. The antenna is low cost and easy to fabricate with additional benefit of being a compact and low-profile structure.

In the next chapter we introduce the survey performed on antennas in the UHF band. The 406 MHz antenna is smaller in wavelength which means the physical size compared to a VHF antenna is smaller. Like VHF antennas, the challenge of designing UHF antennas for the ADFR is the limited size available and the effect on performance by components near active elements. This will be addressed in the next chapter.

Chapter 4

4.0 UHF Antenna Design

The goal of this chapter is to describe the survey done on UHF antennas and obtain knowledge about how they work. The target frequency is 406 MHz. Different design alternatives were investigated to obtain an antenna with the best performance. The antennas considered but not presented here include quadrifilar helix, patch antennas, spiral antennas, and dielectric resonator antennas. For completeness, the references are provided for those antennas not detailed in this thesis. The antennas presented in this section include the turnstile antenna, the Alford-loop-type antenna, and the slotted-loop antenna. After analyzing the different alternatives, the best antenna meeting C/S T.001 requirement is presented with full simulation analysis and measurement results.

4.1 Design Requirement and Consideration

The general electrical performance requirement for the 406 MHz antenna is prescribed by C/S T.001 (First Generation Beacons), C/S T.018 (Second Generation Beacons), Document RTCA/DO-204 Minimum Operational Performance Standards. A summary of these specifications is shown in Table 5.

4.1.1 Mechanical Requirements

The initial available space for the new 406 MHz antenna consisted of the thickness of the four sidewalls of the ELT container. The initial ELT container was 17 inches x 17 inches x 5.8 inches.

Table 5: Minimum requirements based on C/S T.001 (FGB)

Antenna Parameters	Antenna Characteristics	Comments
Frequency	406 MHz	Minimum bandwidth of more than 200 kHz
Radiation Pattern	Hemispherical	Omnidirectional radiation pattern in azimuth
Polarization	Linear or RHCP	Vertical/Horizontal or Right Hand Circular Polarized
Antenna Gain (Azimuth)	-3 dBi to +4 dBi	Over 90% of full 360 degrees azimuth range
Antenna Gain (Elevation)	-3 dBi to +4 dBi	Over 90% of elevation range between 5^{o} < EL < 60^{o}
Gain Variation	≤ 3 dB	-
Antenna VSWR	≤ 1.5:1	50 Ω system

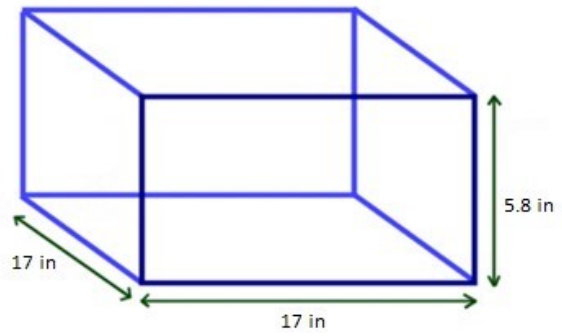

Figure 42: Initial ADFR available volume

As the designed stage matured the mechanical requirements evolved in to a more compact size which required a redesign of the preliminary antenna concept while still meeting the requirements prescribed by C/S T.001.

4.2 Turnstile Antenna

A turnstile antenna, also called crossed dipole, is a type of array antenna. Two identical half-wave dipoles are placed at right angles to each other and are excited 90° out of phase with each other. The antenna can be configured in normal mode or axial mode. In normal mode the antenna radiates horizontally polarized radio waves perpendicular to the plane of the two crossed dipoles, while in axial mode the antenna radiates circularly polarized radiation orthogonal to the plane of the two crossed dipoles [17].

The radiation pattern is omnidirectional within 5% with maximum directivity located at the ends of the elements [18]. When the radiation above the plane of the crossed dipoles is RHCP, below the plane is LHCP. The polarization is determined by the phase of the feed connections. For a directional antenna, only a single beam is wanted. Hence, with a simple axial-mode antenna a flat conducting surface such as a metal screen reflector can be added, a quarter-wavelength behind the crossed elements [17]. The waves in that direction are reflected, and the reflection reverses the polarization sense, so the reflected waves reinforce the forward radiation.

The requirement for the turnstile to function is to ensure each dipole's currents are of equal magnitude and in phase quadrature. This is done with feed-line techniques or by adding reactance in series with the dipoles [18]. A popular method of feeding the two dipoles in a turnstile antenna is to split the RF signal from the transmission line into two equal signals with a two way splitter, then delay one by 90° additional electrical length. Each phase is applied to one of the dipoles. By modifying the length and shape of the dipoles, the combined terminal impedance presented to a single feed-point can achieve pure resistance and yield quadrature currents in each dipole [18], [19]. This method of changing the physical dimensions of the antenna element to yield quadrature currents is known as "turnstile feeding".

The advantages of turnstile antennas include high gain when stacked along a vertical axis, and phased, as shown in Figure 43. If multiple turnstiles antennas are vertically stacked, high gain may be achieved by strengthening the radiation in the desired vertical direction but causes partial cancellation of the radiation in the horizontal direction, resulting in loss of power.

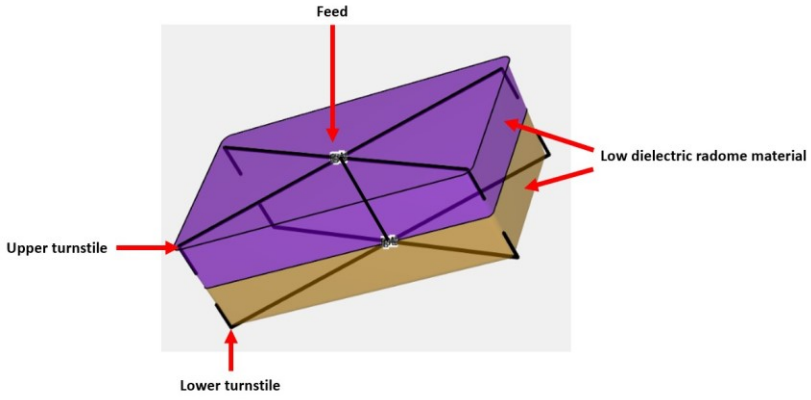

Figure 43: Turnstile antennas fed 90˚ out of phase

Two turnstile antennas a quarter wavelength apart fed 90˚ out of phase, was constructed and simulated. The length of the dipoles was calculated using the method introduced in [17]. Figure 43 shows the two turnstile antennas around a dielectric material representative of the ADFR in which the antenna is expected to be placed.

The simulated 3D pattern is shown in Figure 44. The left pattern shows the total field pattern in free space. The right pattern is when a ground plane is introduced a quarter-wavelength away. The results were promising with a 3 dB bandwidth of 15% at 406 MHz. However, the radiation pattern is very sensitive to ground plane effect and distorts when the ground plane is less than $\lambda/4$ away from the antenna. A shift in the center frequency also occurs, along with an increase in VSWR and a reduction in the power output. For this

reason, this solution was considered not to be a candidate solution for implementing in the ADFR.

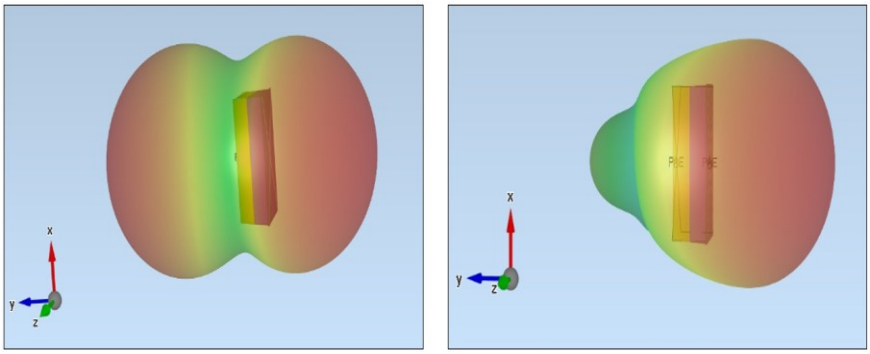

Figure 44: 3D Turnstile total field magnitude pattern

4.3 Alford-Loop Type Antenna

The Alford Loop antenna was first introduced in 1940 by Andrew Alford for the application of a Doppler VHF Omnidirectional Range (DVOR) antenna array for short range navigation systems [20]. It is a horizontally polarized antenna and has the pattern of a vertically polarized dipole antenna making it attractive in the VHF/UHF band. Most RF interference (noise) signals are predominantly vertically polarized so by designing an antenna transmitting in the horizontal plane, the chances of signal interference are minimized. Like the vertical dipole, the Alford-loop radiates in an omnidirectional fashion except it radiates only horizontally polarized waves whereas the dipole radiates only vertically polarized waves.

One of the conditions of C/S T.001 is that the antenna must radiate in elevation angles between 5 and 60 degrees (5 < elevation angle < 60) while obtaining an omnidirectional pattern in the azimuth plane. Figure 45 below illustrates this better.

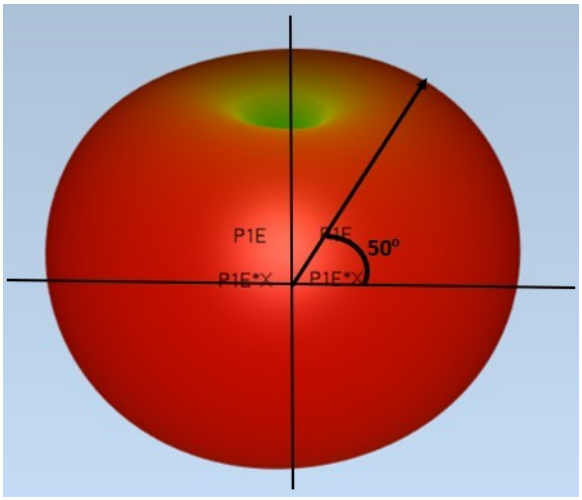

Figure 45: Illustration of radiation pattern requirement in elevation angle

For a reduced size loop antenna, the maximum radiation pattern in the azimuth plane is located both above and below the horizon. Knowing this characteristic, two horizontally oriented loops vertically separated by a quarter-wavelength can be fed 90 degrees out of phase to control the hemisphere for which the radiation is maximum. Depending on which hemisphere of the horizon the antenna is desired to transmit, the switching can be realized by a single-throw-double-pull (SPDT) switch.

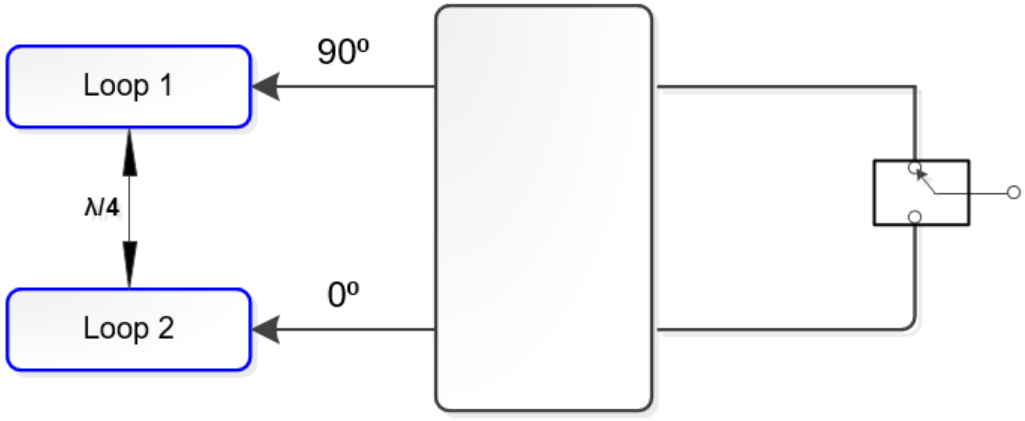

Figure 46: Proposed 406 MHz loop antenna with a switch and quadrature hybrid that allows top or bottom loop to radiate for maximum radiation coverage

4.3.1 Theory of Operation

The Alford loop antenna in Figure 47 was first introduced in [21]. It is made of four half-wave dipole elements folded and arranged so that the elements midsections form a square approximately quarter-wave on each side. It is fed at the terminal [K, K] and the current flowing on the folded-back portions of the elements [BB, DD, CA] flow in opposing directions and therefore they cancel out and contribute very little to the radiated field. Due to its outside loop symmetry, the current distribution on conductors 1, 2, 3 and 4 has the same instantaneous phase travelling along the loop's circumference, consequently, a large electrically loop antenna is achieved with a horizontally polarized omnidirectional pattern.

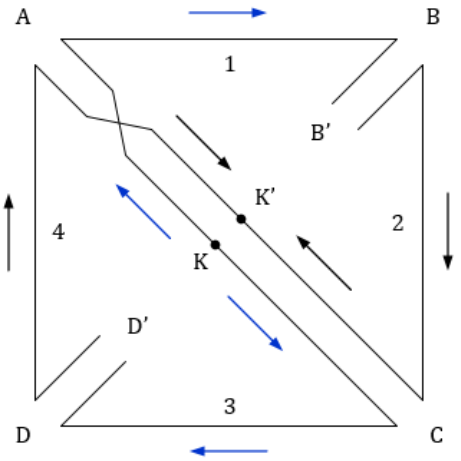

Figure 47: Original Alford loop antenna presented in **[21]**

Field along a Loop Antenna

Since far-field radiation of small loops are independent of shape and only depend on the area of the loop [21], we will consider the Alford-loop as a square-loop as shown in Figure 48 to simplify the analysis.

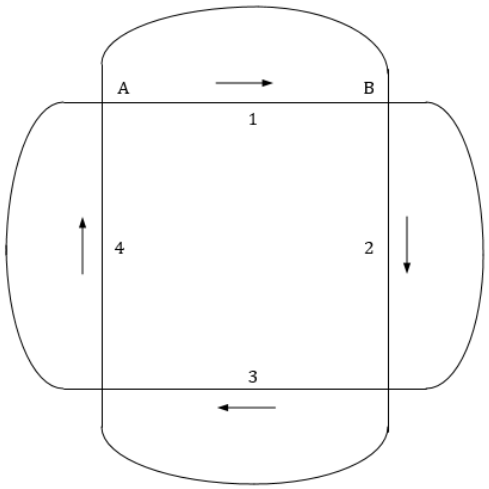

Figure 48: Geometry for a square loop antenna

The magnetic field due to one side of the conductor is approximated in [21] to be:

$$H_1 = \frac{2Io}{rc}\left(\beta l\, sin(\theta)\right)\cos\left(\omega t - rk - \frac{1}{2}kl\right) \tag{41}$$

The above equation is true when the ratio of the length of the loop sides to wavelength (l/λ) is small.

The magnetic field of the loop is a vector sum of all the fields in each of the four sides,

$$\boldsymbol{H} = H_1 + H_2 + H_3 + H_4$$

The total field due to all sides of the loop can be approximated to:

$$\boldsymbol{H} = \frac{8I_o}{rc}\frac{\pi l}{\lambda}\left[sin\alpha\ \sin(\frac{\pi}{\lambda}cos\,\theta) + cos\,\alpha\, sin(\frac{\pi l}{\lambda}cos\,\theta)\right] \tag{42}$$

Assuming (l/λ) is small the magnetic field is further approximated to:

$$\boldsymbol{H} = \frac{8I_o}{rc}\left(\frac{\pi l}{\lambda}\right)^2 cos\beta \tag{43}$$

For a square loop antenna of length L and having a sinusoidal current distribution, the electric field is therefore simply:

$$\boldsymbol{E} = \eta\boldsymbol{H} = \eta\frac{8I_o}{rc}\left(\frac{\pi l}{\lambda}\right)^2 cos\beta \tag{44}$$

The current distributions along the radiating arms are sinusoidal, and the peak occurs at the center of each arm expressed as:

$$I(x) = I_m\ \cos(\beta x) \tag{45}$$

$$I(y) = I_m\ \sin(\beta y) \tag{46}$$

where,

I_m is the current at the center of each conductors
β is the propagation constant

The standing wave on each half-wave dipole (Figure 50) results in current flowing with the same phase at all locations while the voltage is a minimum at the end of the radiating element. Consequently, an equal current illumination in the same direction occurs (Figure 49) in the direction of maximum radiation. With four dipoles center fed in-phase with each other, an electrically large loop antenna can be achieved. Figure 51 shows simulation result for current distribution of a center-fed half-wave dipole showing maximum current at the center of the feedline.

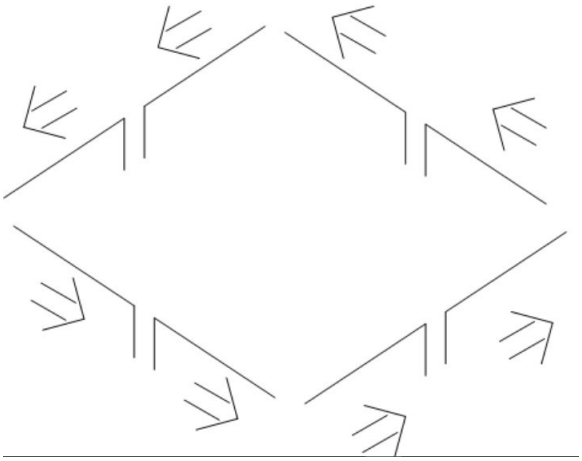

Figure 49: 406 MHz loop antenna made from 4 half-wave dipoles

Provided the antenna is isolated in space and the wire diameter is much smaller than the antenna length L, then the radiation resistance R_r is 73Ω and the reactance X is approximately zero for $L \cong \lambda/2$. The reactance X of a full-wave antenna for which $L \cong \lambda$, as illustrated in Figure 52, is also approximately zero, while the radiation resistance is somewhat greater than 73Ω because it radiates slightly more total power into two hollow cone lobes along the axis.

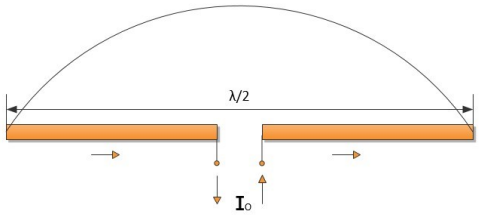

Figure 50: Half wave dipole antenna current distribution

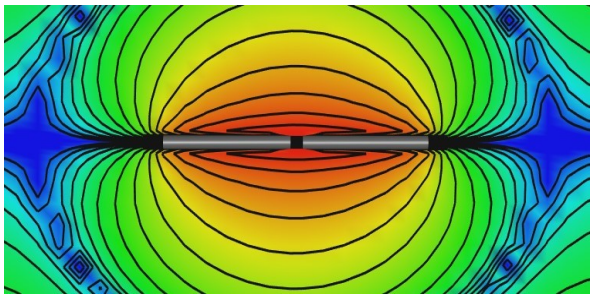

Figure 51: Simulated half-wave dipole antenna current distribution

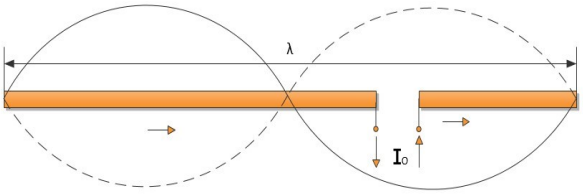

Figure 52: Full wave dipole antenna current distribution

The radiation pattern for the half-wave dipole looks like Figure 53. The radiation from a half-wave dipole is slightly more directive than a full-wave dipole because signals radiated closer to the z-axis along the full wave dipole tend to cancel, particularly when the two ends one-half-wavelength lobes are considered.

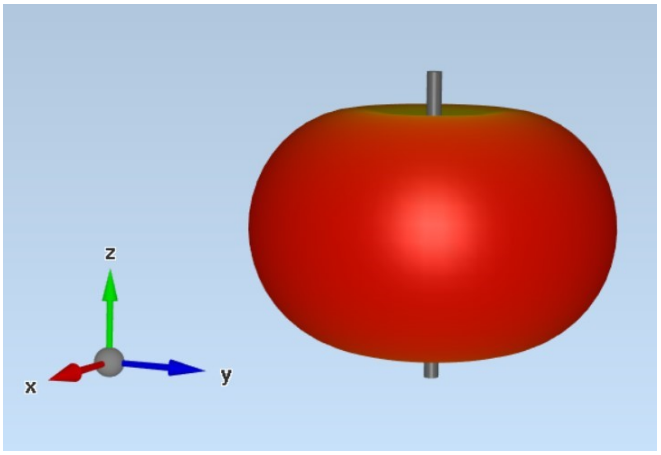

Figure 53: Radiation Pattern of half-wave dipole antenna

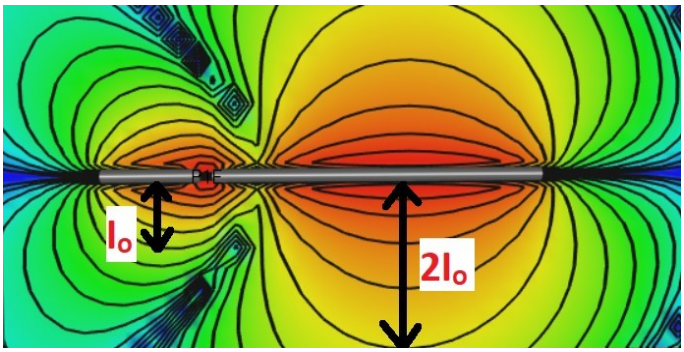

Figure 54: Current distribution on an off-centre dipole antenna

Wire antennas such as the half-wave dipole can be approximated because of the current distribution along the wire is known. As a result, we can easily predict the current distribution of off-centre-fed dipole antennas such as in Figure 54. This antenna is fed a small fraction of a wavelength from one end so that the input current I_o is much smaller than the peak current distribution $2I_o$ one-quarter wavelength from the open-circuit end of the long wire. This current distribution follows directly from the standing wave assumption and the location of the current feed relative to the two ends of the antenna. By placing the feed point even closer to the left-hand end of the antenna, the ratio between the peak current and the drive current can be made even greater than the illustrated ratio of two. Thus, this off-centre-fed antenna exhibits transformer-like qualities. Because most of the power in this antenna will be radiated as if from a half-wavelength dipole carrying $2I_o$, its radiation resistance is greater than that of a center-fed half-wave dipole, although its reactance X is capacitive as a result of the excessive electric energy stored to the left of the current null near the feed point.

The TEM model for current distribution breaks down when different parts of a wire antenna system interact strongly, or when radiation itself begins to alter the current distribution. For example, the long-wire antenna illustrated in Figure 55 radiates sufficiently well that the TEM wave travelling from the feed point to the right toward the long end of the antenna decays approximately exponentially. The result is a standing wave

in the one-half wavelength segment at the left end, a travelling wave portion to the right, and a standing wave portion near the right-hand end where the decaying wave is reflected. This is shown in Figure 56 with successive nodes and antinodes of current along the wire in the form of a pure standing wave. It is worthwhile noting that the longer the dipole gets the more of these nodes and antinodes are formed with different radiation pattern.

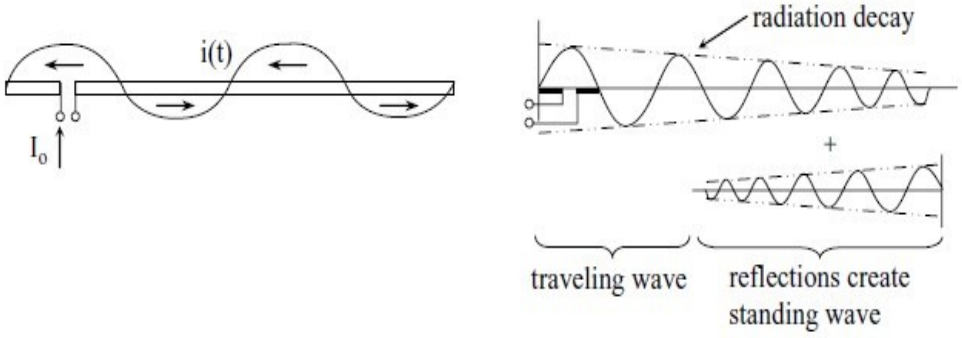

Figure 55: Current distribution on an off-centre long dipole antenna **[22]**

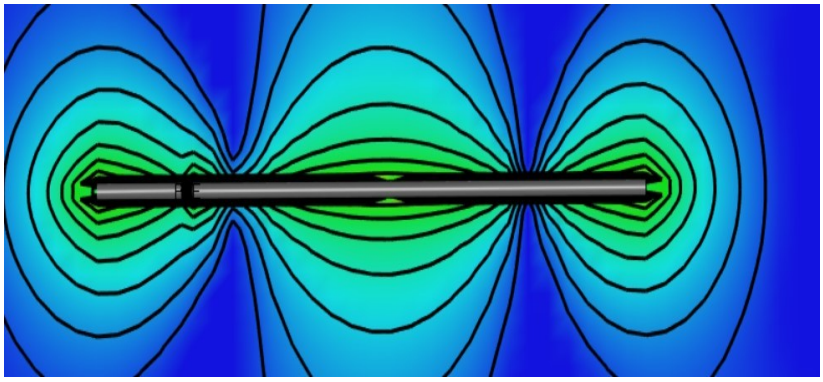

Figure 56: Simulated current distribution on an off-centre long dipole antenna

4.3.2 Single 406 MHz Alford-Loop-Type Antenna

The preliminary proposed antenna adopts the Alford-loop concept designed to transmit at 406 MHz with a wavelength of λ = 73.9 cm (29.1 in). Each side of the loop is therefore $\frac{\lambda}{2} = 37\ cm$ (14.6 in) made with a half-wave dipole antenna center fed in phase with each

other and placed on top of fibreglass with a dielectric constant of 4.9. The simulated structure is shown in Figure 57.

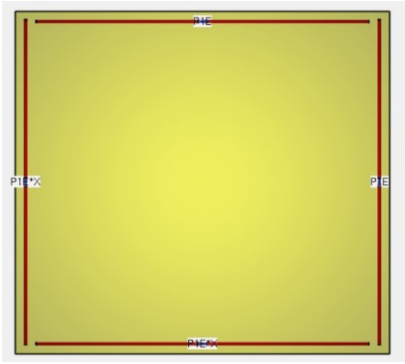

Figure 57: Simulated 406 MHz loop antenna structure

Simulations were performed with EMPIRE XPU. The radiation pattern is shown in Figure 58 below. The results show the expected omnidirectional pattern of the loop looking straight up normal to the surface where the null occurs.

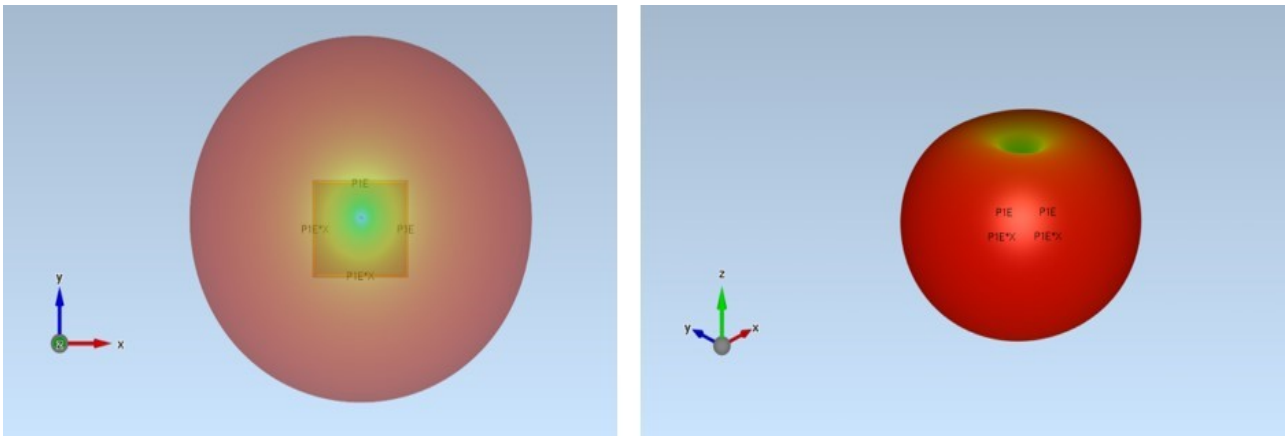

Figure 58: Radiation of 406 MHz loop antenna in the xy-plane (left) and 3D radiation pattern (right)

The polar plots are shown in Figure 59 for the antenna performance in free space (left) and for the antenna performance with ground plane a quarter-wave below the loop (right). The

ground plane effect is expected to reflect the electric field from a conductive surface and superimpose with the primary radiated fields giving a pattern mostly directed above the horizon.

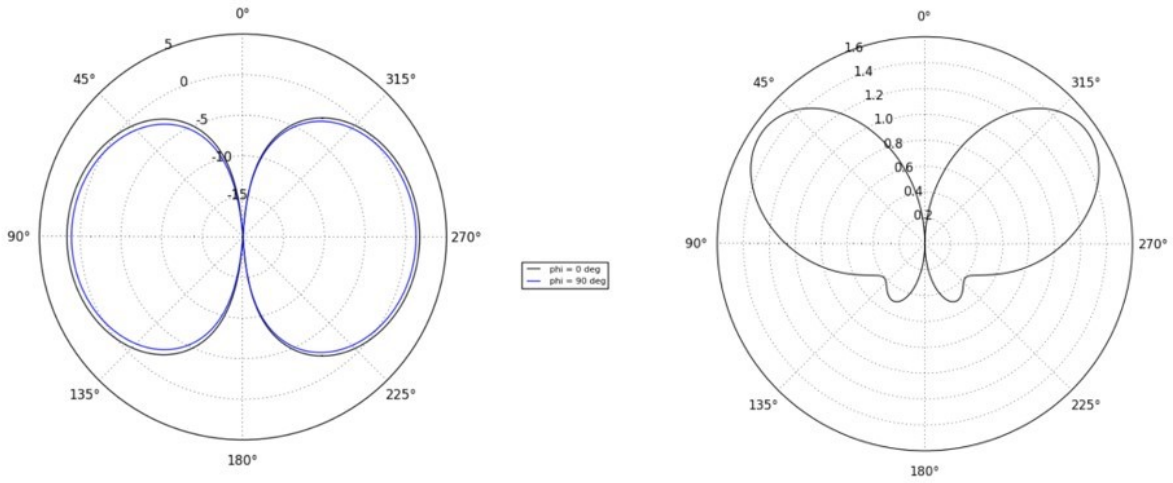

Figure 59: Polar plot of single Alford loop antenna in free space (left) and with $\lambda/4$ ground plane (right)

The simulated results in Figure 61 and Figure 62 show the return loss was strong at 406 MHz with an impedance of about 53Ω. The peak power was focused at about 40 degrees above the horizon shown in Figure 60.

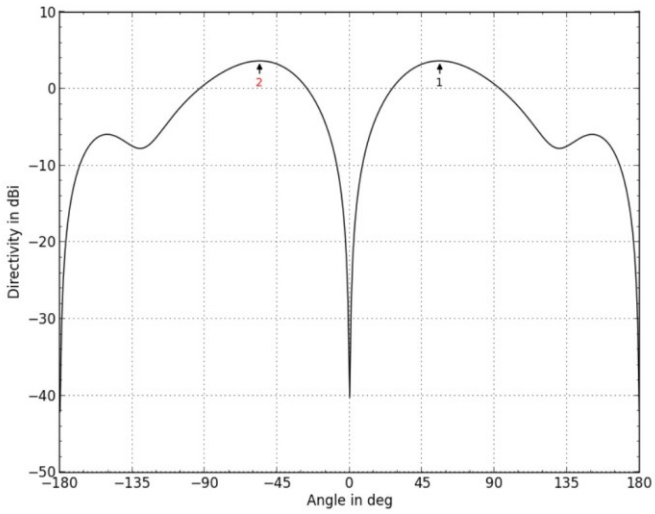

Figure 60: Radiation pattern of single Alford loop antenna. Maximum directivity at about 40 degrees above horizon

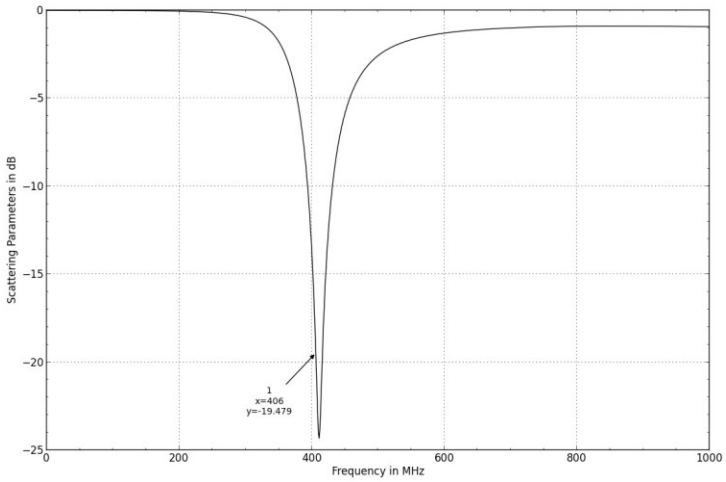

Figure 61: Return loss (S11) for a single Alford-loop-type antenna

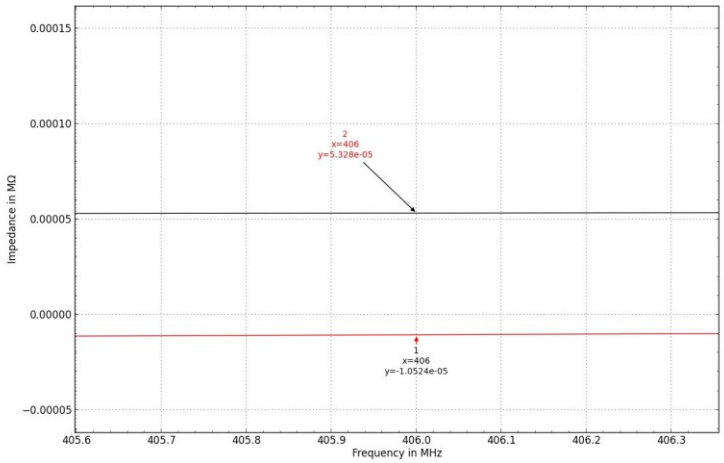

Figure 62: Simulated Impedance for a single Alford-loop-type antenna

The results suggest that a single Alford-loop-type antenna composed of 4 dipoles is a feasible solution for transmission of 406 MHz signal above the horizon. To transmit at the lower side of the horizon, a second loop antenna separated by half-wavelength from the top loop is placed 90 degrees out of phase as shown in Figure 63.

Maximizing Elevation Beam Coverage with Two 406 MHz Alford-Loop type Antenna

The simulated structure of the two-loop antenna concept is shown in Figure 63. The radiation pattern in Figure 64 shows the peak gain when the top loop antenna is turned on while the bottom loop is off (green) and when the bottom loop in on while the top is turned off (black). This is to simulate an ADFR after deployment; it could land in either orientation, up-side down or vice versa. The up squinted and down squinted beams are +/- 45 degrees and +/- 135 degrees respectively, each representing a cone like pattern, one looking up and the other looking down.

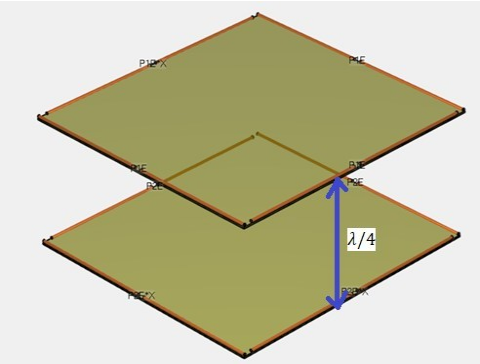

Figure 63: Double loop 406 MHz antenna structure

More importantly, the ratio of the dominant lobe (above the horizon) to its image location (below the horizon) is 6 dB; 4 times the power is directed upwards than downwards.

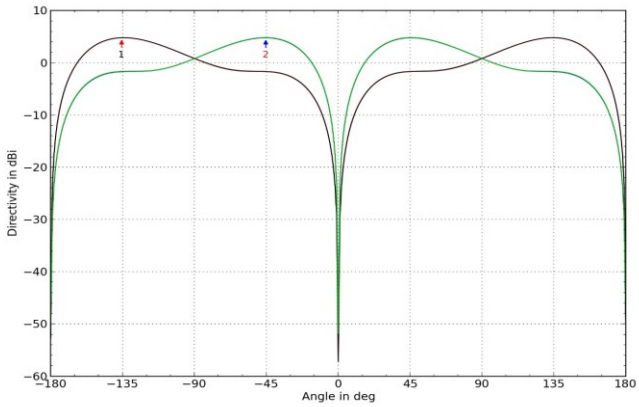

Figure 64: Double-loop Alford-type antenna radiation pattern

Measured Results

A prototype structure in Figure 65 was constructed consisting of a wooden frame with initial dimensions of the ELT container (17 x 17 x 5.8 inches). The structure consists of a commercial quadrature hybrid (to obtain the 0 / 90 degrees or 90 / 0 degrees phase relationship from the two Alford type loops) and two 4-way power dividers (to connect to each of the four dipoles making up each of the Alford type loops). In place of the SPDT switch which selects the orientation of the radiating loop antenna, the output cable was reconnected to one of the two quadrature hybrid outputs.

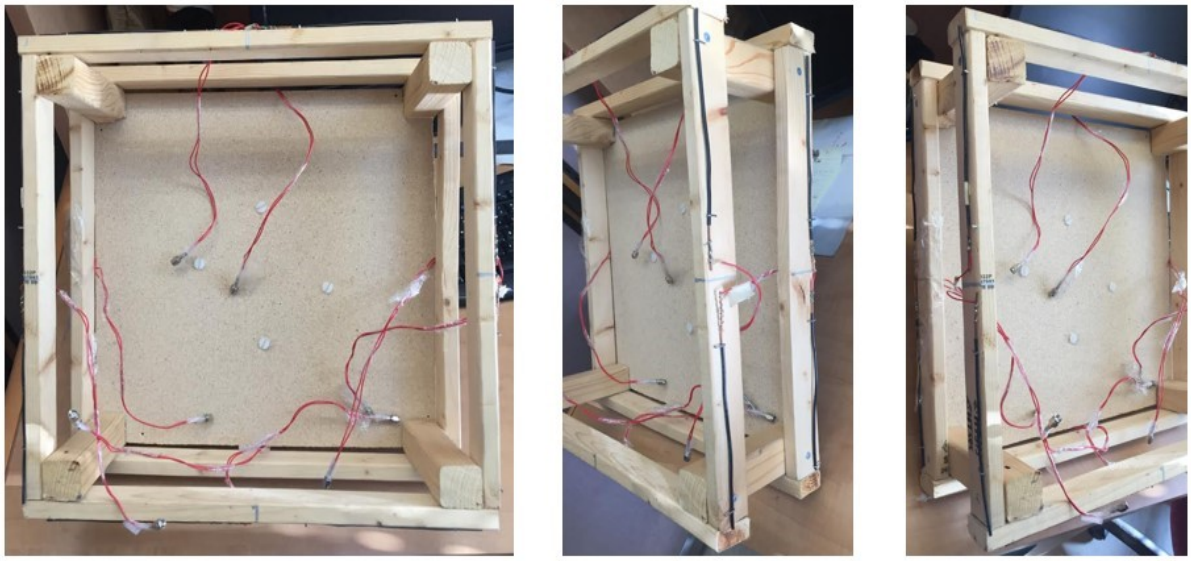

Figure 65: Fabricated structure of the double-loop Alford-type antenna

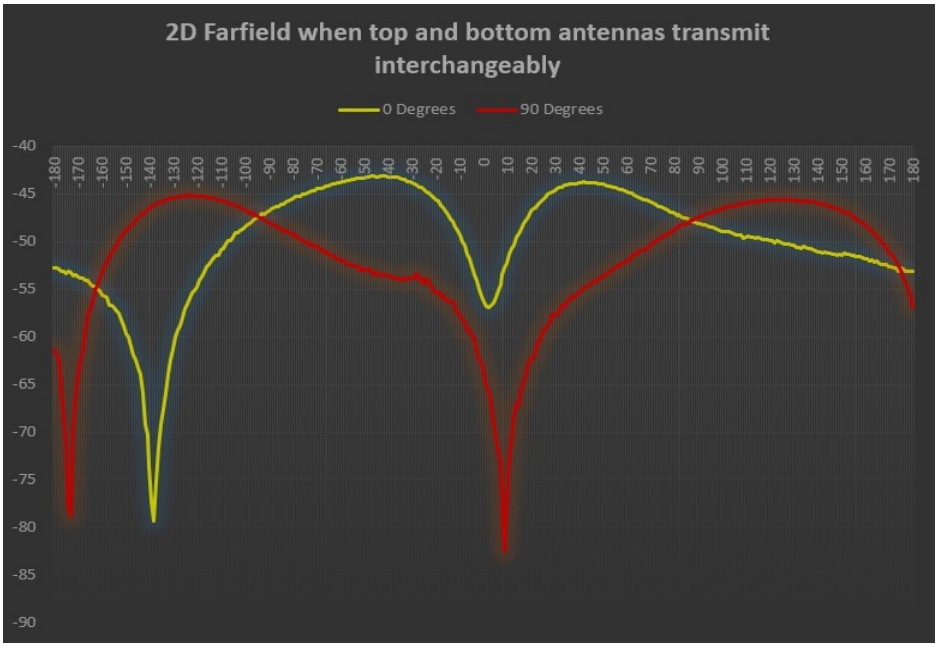

Figure 66: Double-loop Alford-type antenna radiation pattern

The measured elevation patterns are shown in Figure 66. Here 0 degrees represents the normal to the earth's surface (straight up). As in the simulations, the up-tilted beam forms its maximum near 45 degrees, while the down-tilted beam forms its maximum near 135 degrees.

4.3.3 Corner Folded Alford-Type-Loop Antenna Structure

As volume requirements changed, the size of the antenna needed to also change. To accommodate the smaller volume, the antenna needed to be smaller hence folded technique (Figure 67) was employed to minimize the area of the loop. It was shown above that by folding the dipole at the corner of the square the current distribution does not get disrupted since the current on the folded section cancel out. By feeding at the center of sides, the current maximum will be at the center and provides a more symmetrical current illumination in the azimuth plane, which is a lot better than a conventional Alford antenna. With this knowledge, the loop in Figure 67 was simulated with side length of $\frac{\lambda}{3} = 25\ cm\ (9.8\ in)$ while the length of the folded portion of the loop was about $\frac{\lambda}{6} = 13cm\ (5.1\ in)$, reducing the length of the Alford-type-loop by about 50 percent.

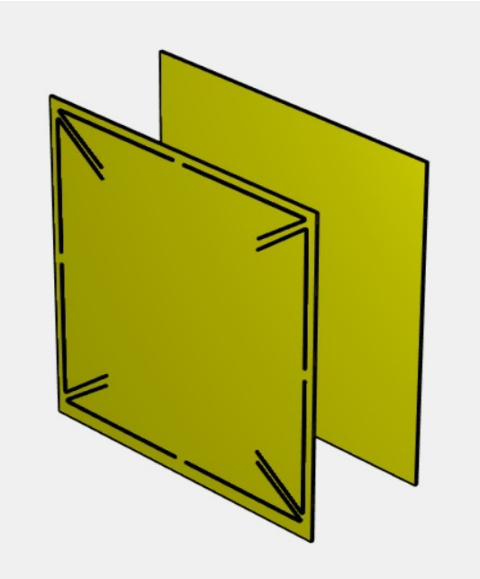

Figure 67: Corner Folded Alford-type loop antenna

The simulation results for the case where the loop antenna is folded at each corner of the square show identical results as for the loop antenna without its sides folded. This is encouraging since it confirmed our theory that the phase current along the loop remains constant, as shown in Figure 68.

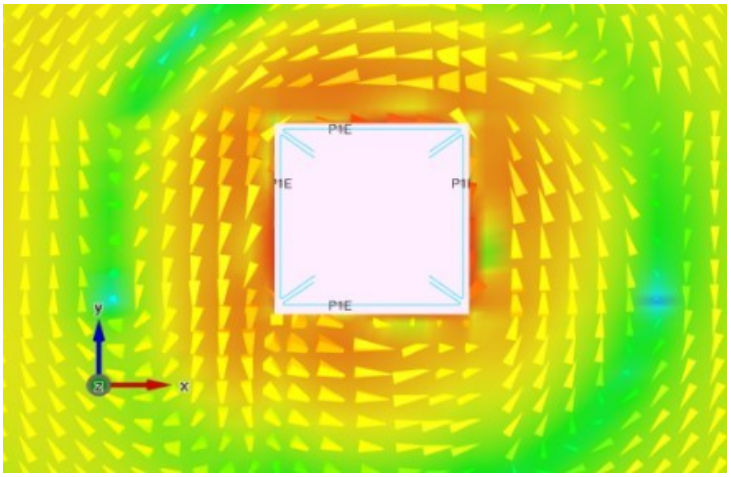

Figure 68: Surface Current density of the corner folded antenna

The dipole like pattern is also shown in Figure 69 with the formation of nulls by individual corner elements. Figure 70 and Figure 71 show the simulated results of the radiation pattern in the farfield.

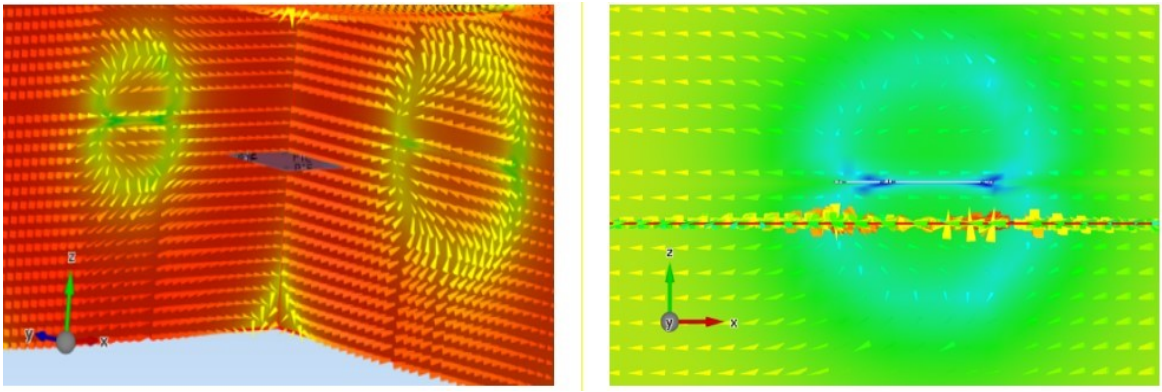

Figure 69: 2D and 3D view of dipole like pattern of corner folded Alford-loop type antenna

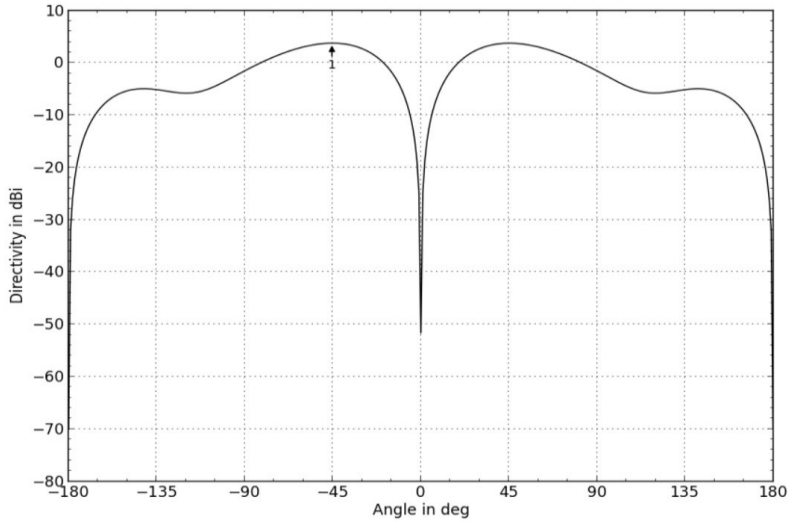

Figure 70: Corner folded Alford-loop-type simulated 2D pattern

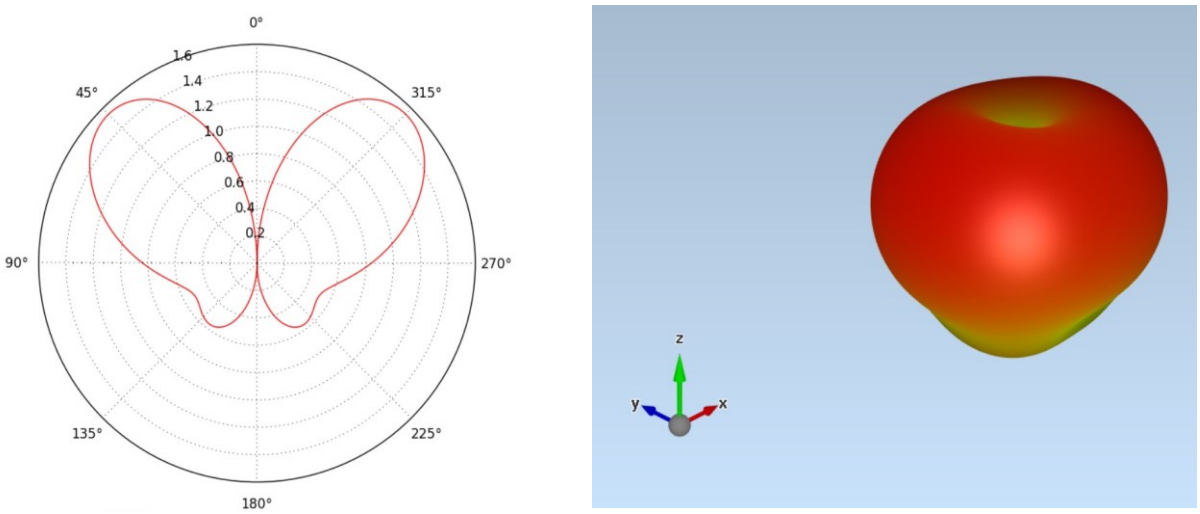

Figure 71: Corner folded Alford-loop-type simulated polar plot (left) and 3D pattern (right)

This antenna was fabricated at Metaplast Circuits in Ottawa and tested inside DRS TCL's anechoic chamber. 1 oz. of copper element was etched on the PCB panel made of FR4. Each of the four dipole elements was fed with an RG 316 coaxial cable with SMA connector. The four feeds were combined in a 4-to-1 combiner from Mini-Circuits (ZFSC-4-1W-S+). See Figure 72.

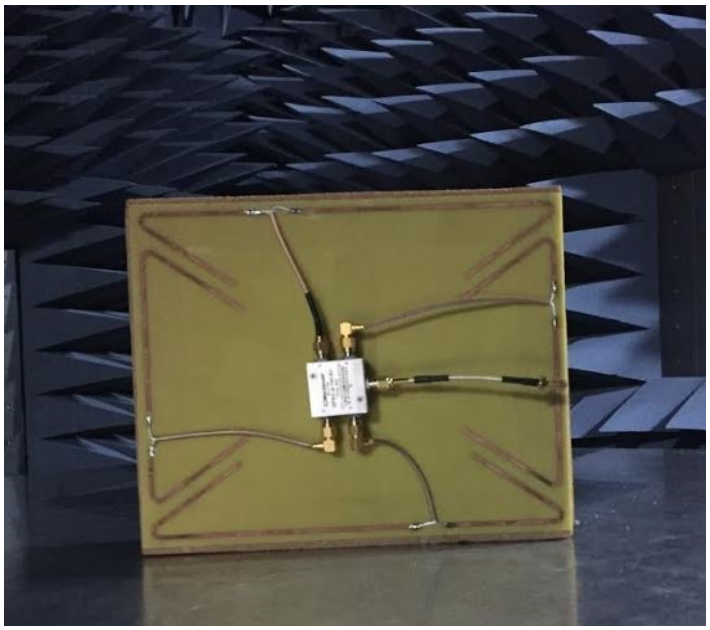

Figure 72: Fabricated corner folded Alford-loop-type antenna

The measured radiation pattern for elevation angles at 10^o and 20^o is shown in Figure 74. The results are compared to the simulated pattern shown in Figure 73. The measured radiation pattern was omnidirectional within 3 dB which was also noticed with the simulated results. The measured directivity however was down 6 dB compared to that of the simulation. This is due to the antenna's close proximity to the finite ground plane which might have detuned the antenna's resonant frequency. Loss due to the 4-to-1 RF combiner might also contribute to the poor performance. Loss varies depending upon the phase and amplitude relationship of the signals being combined [23]. For example, in a 2 way 0^o power splitter/combiner (Figure 75), if the two input signals are equal in amplitude and are in-phase then the loss is zero. However, if the signals are 180^o out-of-phase the loss is infinite and, if the two signals are at different frequencies, the loss will equal the resistive loss.

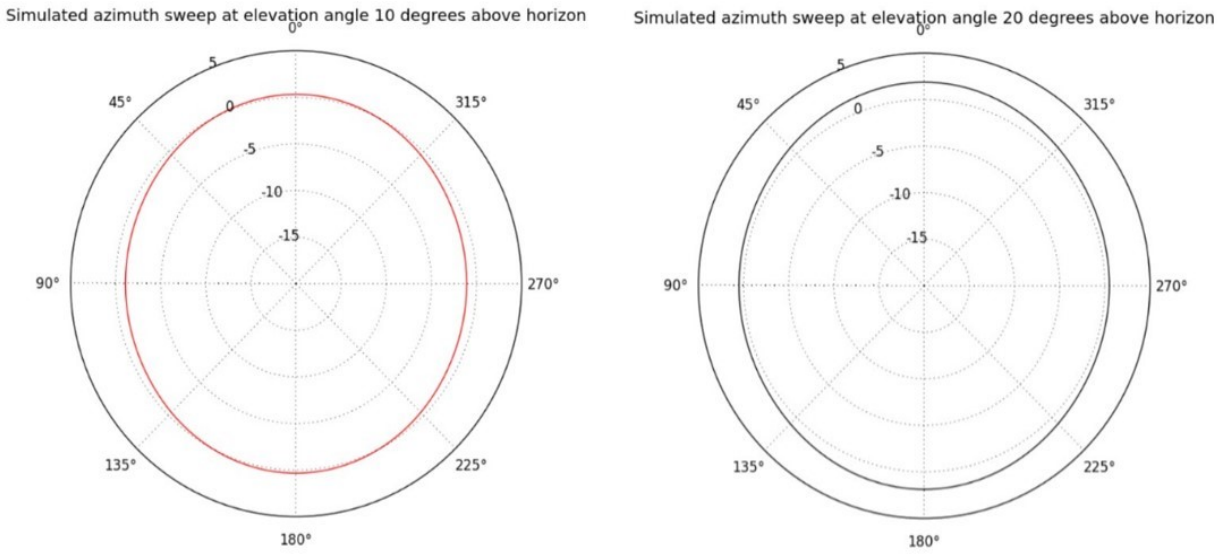

Figure 73: Simulated pattern at 10^o (left) 20^o (right) elevation angles

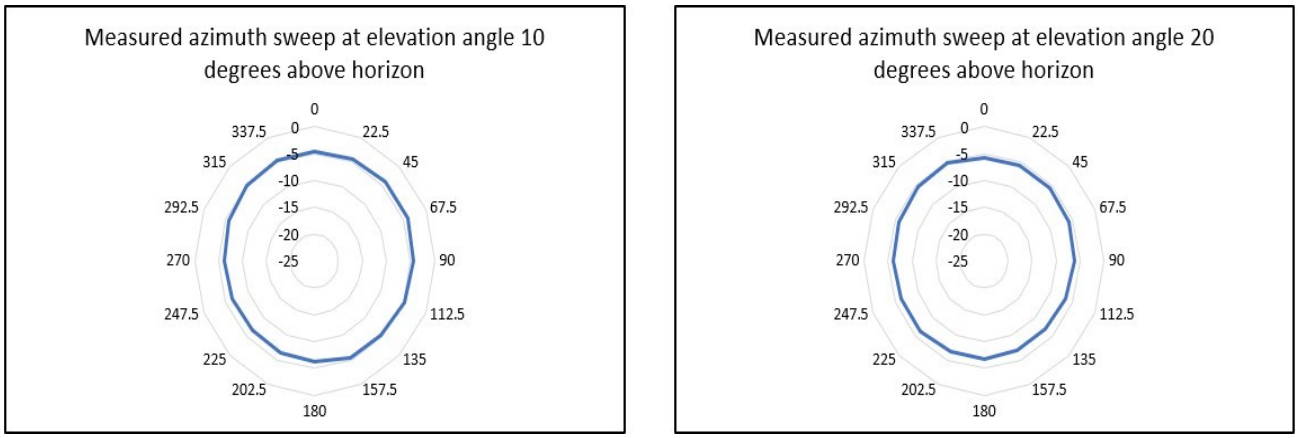

Figure 74: Measured pattern at 10^o (left) 20^o (right) elevation angles

The power combiner will also exhibit isolation between the input ports. The amount of isolation will depend upon the impedance termination at the combiner output or sum port. For example, in the 2 way 0^o power splitter/combiner of Figure 75, if port S is open then the isolation between ports A and B would be 6 dB. If port S is terminated by matched

impedance (for maximum power transfer) then the isolation between ports A and B would ideally be infinite.

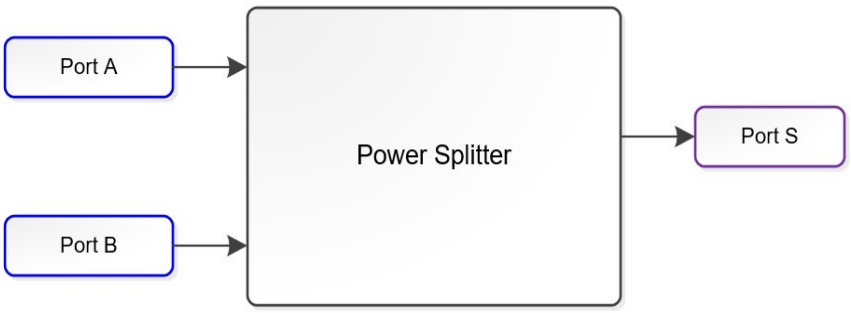

Figure 75: Two-port power divider

4.3.4 Double-slotted Loop Antenna

Previously, in Chapter 3, slot antennas have been discussed. One of the many benefits of slot antennas is that they are low profile and easy to manufacture. Loop antennas are directional and do not require ground plane. In this section, the benefits of loop antennas will be discussed, one of which is omnidirectionality. Now, if these two attributes were to be combined, that is, the slot and loop antenna, then the result could yield an electrically small 'Slotted-loop' antenna with superb performance.

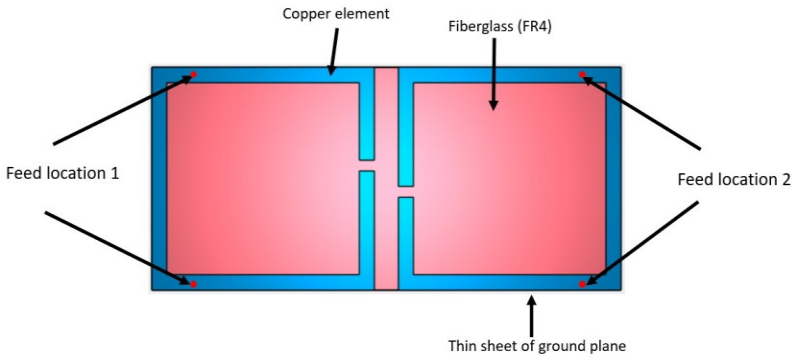

Figure 76: Slotted-loop antenna with two loops fed in phase

Simulations were performed on a rectangular slotted-loop. First, a single rectangular slotted-loop was simulated to resonate at the UHF frequency. The loop width was varied from a narrow to a wider size that approached approximately 3 inches (7.5 cm). To determine the length, slot radiator theory was utilized, which is $\frac{\lambda}{2}$ at the frequency of interest, but in practice the dimension reduces by a factor of the square root of effective dielectric constant (ϵ_{eff}), that is:

$$\lambda_{eff} = \frac{\lambda}{\sqrt{\epsilon_{eff}}} \tag{47}$$

where,

ϵ_{eff} is the effective dielectric constant

λ_{eff} is the effective wavelength

The antenna feed of this model consists of two coaxial lines soldered across each of the slotted-loop width in a location close to the end of the loop, which has been found experimentally to achieve the optimum impedance matching to 50 Ω. After much iteration, the proper slot location was found which yielded an omnidirectional pattern and the model in Figure 76 was developed. The antenna is tuned over a range of frequencies by increasing the narrow gap of each loop.

The results in Figure 78, Figure 79, andFigure 81 are compared with that of a fabricated antenna presented in Figure 77.

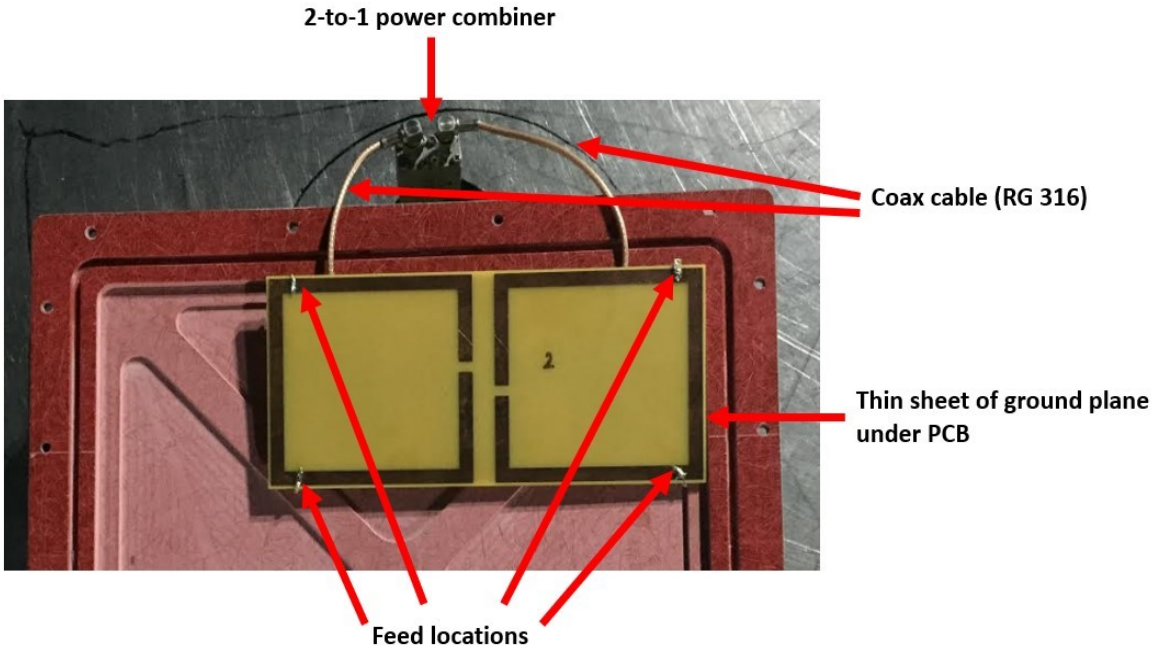

Figure 77: Fabricated slotted-loop antenna with two loops fed in phase

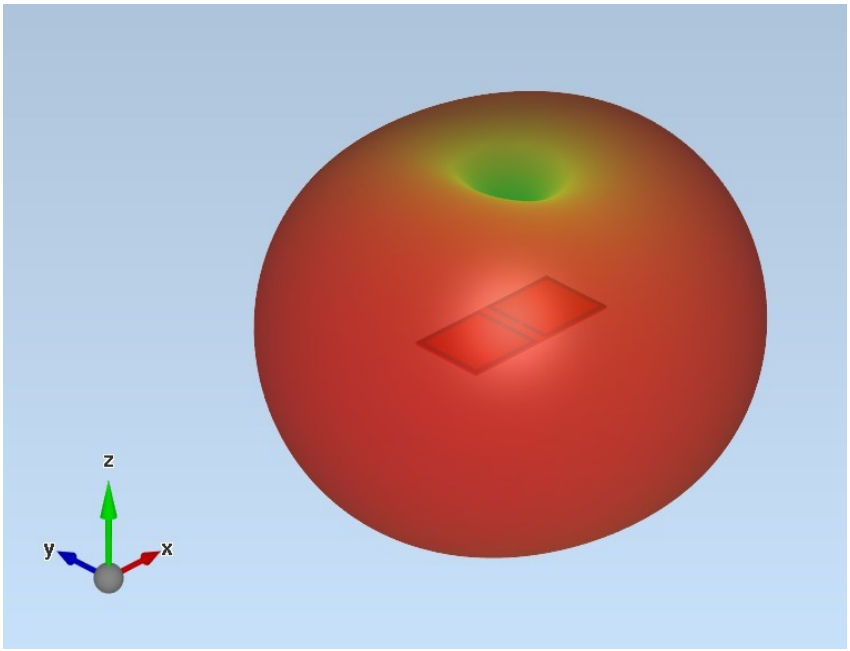

Figure 78: Simulated radiation pattern of slotted-loop antenna with two loops fed in phase

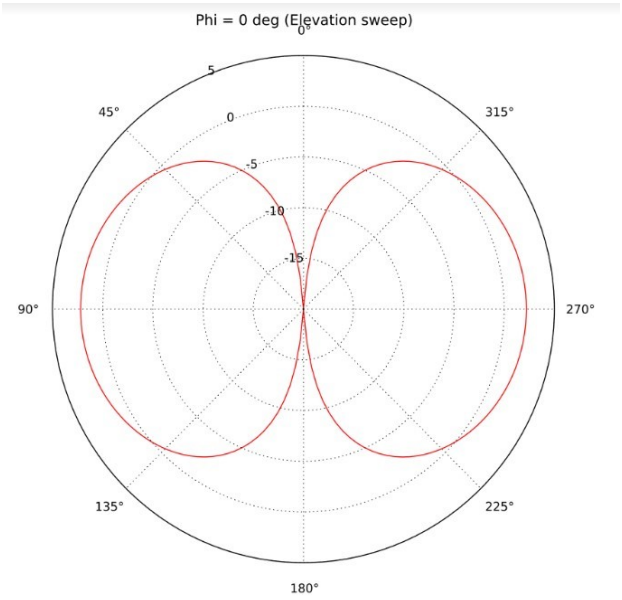

Figure 79: Simulated elevation sweep of slotted-loop antenna with two loops fed in phase

Figure 81 shows 2D farfield plot when the antenna is rotated in the horizontal plane. It shows an omnidirectional pattern with an average directivity of 2 dBi in azimuth. The fabricated antenna measurement agrees with the simulation as shown in Figure 80 (left), with an average directivity of 1.8 dBi. Here, the discrepancy can be attributed to measurement error within the chamber environment.

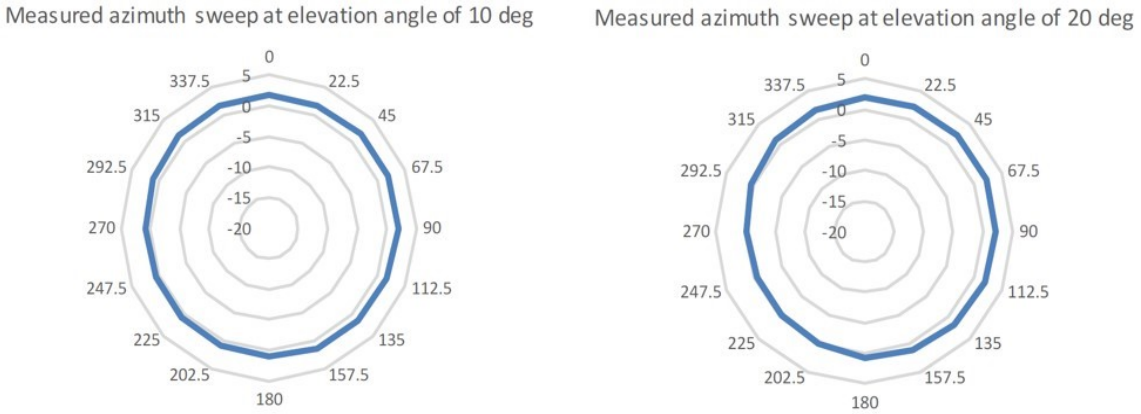

Figure 80: Measured azimuth sweep of slotted-loop antenna at elevation angle of 10^o (left) and 20^o (right)

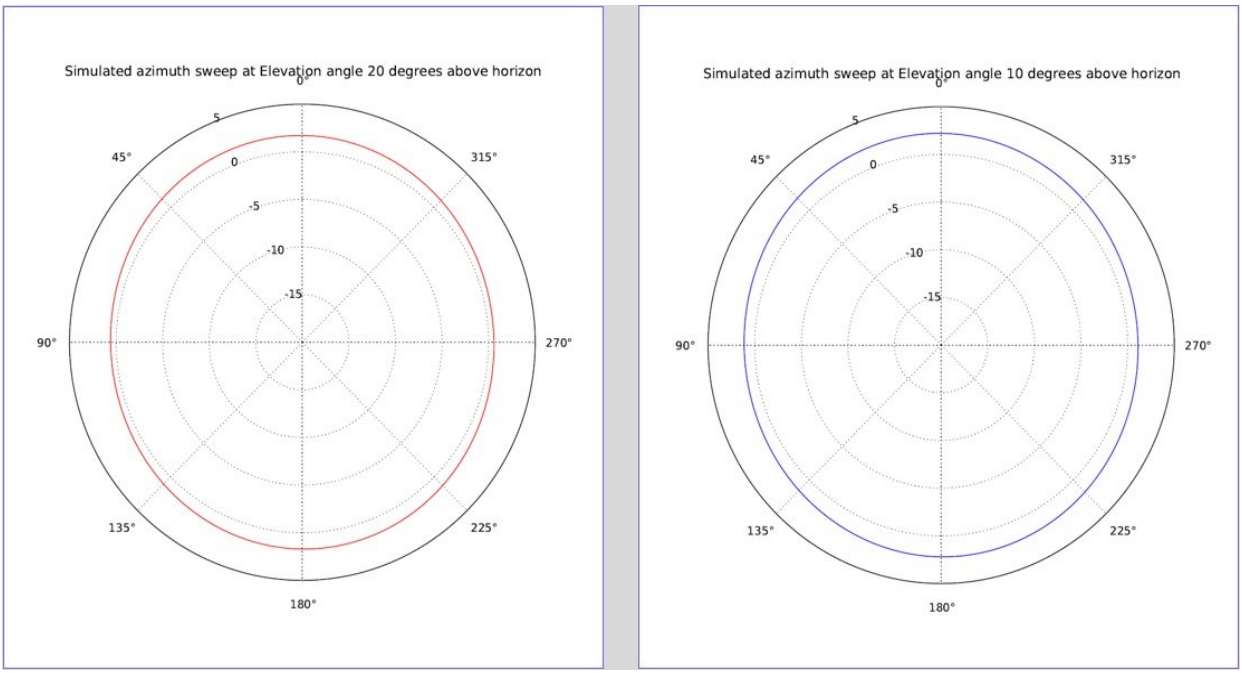

Figure 81: Simulated azimuth sweep of slotted-loop antenna at elevation angle of 10^o (left) and 20^o (right)

The same relationship is observed at higher elevation angles. Figure 81 (right) is the simulated pattern at 20 degrees elevation angle above the horizon, which corresponds to the fabricated antenna in Figure 80 (right), within a 0.5 dB difference. Higher elevation measurements were not taken because the anechoic chamber was not equipped to measure higher elevations. But with the data obtained we can conclude that the slotted-loop antenna is an attractive solution when robust spherical coverage is required in elevation angles and hemispherical coverage in the azimuth plane.

4.4 Chapter Summary

A survey of antennas in the UHF band was done to select the best antenna candidate to integrate with the ADFR. The UHF band was a little forgiving in that the wavelength compared to VHF antennas is lower which makes the physical size of the antenna element smaller. We began by stating that the monopole (whip) antenna is the simplest and effective way to transmit in the UHF/VHF frequency bands. However, since it requires a ground plane to radiate it was considered not to be a feasible option to implement in the ADFR. It is worth noting that there is currently active research in this area and the general consensus is that there is a basic trade-off between the bandwidth of the antenna element and the achievable VSWR.

A variant of an Alford-loop antenna was introduced and shown to have an omnidirectional pattern in the horizontal plane. Electromagnetic simulations were performed using a professional tool by EMPIRE XPU and multiple antennas were fabricated to achieve a final working design. The theory on the original Alford-loop antenna was first summarized to understand the current design. A working prototype was built with 4 dipoles ($\frac{\lambda}{2}$) and the concept of switching the phase relationship of signals illuminating two vertically stacked loop antennas was proven. To minimize the size of the antenna, the corner folded Alford-type-loop antenna was introduced. This antenna proved, both in simulation and measurement, that the current travelling at the corner of the loops cancel out leaving the total loop to instantaneously travel in the same direction. However, measured results showed a 6 dB margin between the predicted and measured gain, which was mainly attributed to finite ground plane effect on the transmitting antenna, as well as splitter loss contributed by the 4-to-1 combiner. The double-slotted loop was introduced, and performance presented both in simulation and measurement. The results showed agreement between simulated and measured results proving the combination of slot and loop antennas to be effective.

Chapter 5

5.1 Conclusion and Future Work

5.1.1 Conclusion

The goal of this thesis was to design UHF/VHF passive antennas that can be integrated to an ELT beacon. Vertical polarization was achieved for both UHF and VHF antennas with a hemispherical radiation pattern for all azimuth angles and elevation angles between 10° and 20°. A compact low profile folded slot antenna has been proposed for the 121.5 MHz frequency using the principles of slot radiators as half-wavelength resonator. An omnidirectional characteristic was achieved within a 3 dB margin. Sensitivity analysis was performed on the feed network of the folded slot antenna to optimize impedance while maintaining sufficient bandwidth.

The 406 MHz antenna exhibits gain over the monopole for elevation angles between 10° and 20°, which translates to a gain of approximately 2 dBi over a theoretical isotropic radiator. A size reduction of about 50% has been achieved by folding the corners of the loop while maintaining the phase current along the loop constant. A novel slotted loop antenna was proposed using the principles of the slot antenna and the conventional Alford loop. The antenna is impedance matched by sliding the feed along the loop and tuned over a range of frequencies by increasing the gap of each loop while maintaining omnidirectionality in the horizontal plane. This antenna will fit in different type of volumes that carry 406 MHz emergency beacons. The antenna can also be utilized in other application, if the dimensions are modified to accommodate the UHF frequency band.

Some environmental requirements such as antenna performance under extreme temperatures (-55 °C to 85 °C) and antenna characteristics such as sensitivities to local

obstructions have been investigated. However, advanced tests are required to finalize the antenna evaluation of the ADFR floating in water while the effects of system elements such as the transmitter, recorder, and battery packs are included.

5.1.2 Future Work

This thesis provides the opportunity of continuing research to meet Second Generation Beacons (SGBs) requirements since a foundation has been established for the First Generation Beacons. As the due dates for implementing SGBs are fast approaching, a good solution such as employing conformal structures as part of a solution might reveal additional advantages in meeting requirements.

Conformal antennas are introduced in Appendix A and their advantage to antenna performance was emphasized. Conformal antennas are antennas that are mounted to a surface of an object and follow the shape of the structure. Background theory on a singly curved surface is presented. Simulation was done with a circularly polarized antenna with a dipole-like radiation pattern embedded on a curved surface of similar dielectric materials and compared to the antenna in free space. The results show the radiation pattern that looks more like that of a patch and not the dipole like pattern of the antenna in free space.

References

[1] Airbus, "Airbus.com," [Online]. Available: http://www.airbus.com/newsroom/press-releases/en/2017/06/airbus-launches-new-fixed-and-deployable-flight-recorders-for-it.html. [Accessed 20 April 2018].

[2] M. Tooley and D. Wyatt (2011). Aircraft communications and navigation systems. Abingdon, Oxon: Routledge.

[3] Forces.gc.ca, “Defence Acquisition Guide 2016”. [online] Available at: http://www.forces.gc.ca/en/business-defence-acquisition-guide-2016/joint-and-other-systems-78.page [Accessed 23 Apr. 2018].

[4] Cospas-Sarsat Secretariat. Specification for Cospas-Sarsat 406 MHz Distress Beacons. C/S T.001, Issue 4 - Revision 2, February 2018.

[5] "RTCA/DO-183 Minimum Operational Performance Standards for Emergency Locator Transmitters Operating on 121.5 and 243 MHz.," May 13, 1983.

[6] "ED-62A - MOPS for Aircraft Emergency Locator Transmitters (406 MHz and 121.5 MHz (Optional 243 MHz).," Feb 2009

[7] "IEEE Standard Definitions of Terms for Antennas.," IEEE Std 145-1993, vol., no., pp.i, 1993. doi: 10.1109/IEEESTD.1993.119664.

[8] A. C. Aznar, Antenas. 2nd ed. Barcelona: Universidad Politécnica de Cataluña, p.19, 2009.

[9] C. Balanis, Antenna theory. 4th ed. Hoboken, New Jersey: Wiley, 2016.

[10] R. Straw, The ARRL antenna book. Newington, Conn.: American Radio Relay League, 2000.

[11] D. Pozar, Microwave and RF wireless systems, 3rd ed., New York: J. Wiley & Sons, 2001.

[12] W. Stutzman, and G. Thiele, Antenna theory and design. 3rd ed. Hoboken, NJ: Wiley, 2013.

[13] A. Petosa, “*Course notes: Elec 5607 - Antenna Engineering Winter 2016".*

[14] D. Pozar, Microwave and RF wireless systems. 3rd ed. New York: J. Wiley & Sons, 2001.

[15] E. Jordan, and K. Balmain, Electromagnetic waves and radiating systems. 2nd ed. Englewood Cliffs, N.J.: Prentice-Hall, 1968.

[16] W.L. Weeks, Electromagnetic Theory for Engineering Applications 1st ed. Hoboken, NJ: Wiley, 1966.

[17] T. Milligan, Modern antenna design. 2nd ed. Hoboken, N.J.: IEEE Press, pp.231–237, 1998.

[18] J. Kraus, and R. Marhefka, Antennas. 2nd ed. Boston, Mass.: McGraw-Hill, pp.726–729, 2003.

[19] F. P. Martin, L. H. Kellogg, “Antenna [Missile]”. US2823381A, 1952.

[20] Z. Chen, D. Liu, H. Nakano, X. Qing, and T. Zwick, Handbook of Antenna Technologies. Singapore: Springer, pp.1415-1478, 2016.

[21] A. Alford and A. G. Kandoian, “Ultra-high frequency loop antenna,” Trans. AIEE, vol. 59, pp. 843–848, 1940.

[22] F. Ulaby, E. Michielssen, and U. Ravaioli, Fundamentals of applied electromagnetics. 6th ed. Boston: Prentice Hall, 2010.

[23] MiniCircuits, "Understanding Power Splitters," [Online]. Available: https://ww2.minicircuits.com/app/AN10-006.pdf. [Accessed 12 03 2018].

[24] L. Josefsson and P. Persson, “Conformal Array Antenna Theory and Design”, Wiley-IEEE Press, March 2006. pp. 1-5, 230-238, 265-302.

[25] K.-M. Luk and W.-Y. Tam, “Patch Antennas on a Spherical Body”, IEEE Proceedings, Vol. 138, No. 1, February 1991.

[26] K. Wong, “Design of Nonplanar Microstrip Antennas and Transmission Lines”, John Wiley & Sons, 1999.

[27] M. d. C. R. González, "ANALYSIS OF CONFORMAL ANTENNAS FOR AVIONICS APPLICATIONS," Masters Thesis, Chalmers University of Technology, 2007.

[28] F. Lumini, L. Cividanes and J.C.S. Lacava, “Computer Aided Design Algorithm for Singly Fed Circularly Polarized Rectangular Microstrip Patch Antennas”, Int J RF and Microwave CAE, vol. 9, No. 1, pp. 32-41, Jan. 1999.

[29] W. F. Richards, Y.T. Lo and D. D. Harrison, “An Improved Theory for Microstrip antennas and applications”, IEEE Trans. of Antennas Prop., vol. 29, pp. 38-46, Jan. 1981.

[30] M. S. Herzog, “Radiation pattern calculation for missile radomes in the near field of an antenna”. Masters Thesis, Naval Postgraduate School, Monterey California, 1996.

[31] Rfbeam.ch, "RADOME (Radar Enclosure)," [Online]. Available: https://www.rfbeam.ch/files/products/12/downloads/AN-03-Radome.pdf. [Accessed 15 03 2018].

[32] www.nasa.gov, "COSPAS-SARSAT Search and Rescue System," [Online]. Available: https://www.nasa.gov/centers/goddard/pdf/105930main_cospas.pdf. [Accessed 19 01 2018].

[33] "Sarsat.Noaa.gov," [Online]. Available: http://www.sarsat.noaa.gov/SCW%202017_files/SAR_2017_SARSAT%20Overview_Feb28.pdf. [Accessed 15 03 2018].

[34] Z. Ryndova, Cospas-Sarsat System - International COSPAS-SARSAT. [online] Cospas-sarsat.int. Available at: https://www.cospas-sarsat.int/en/system-overview/cospas-sarsat-system [Accessed 23 Apr. 2018].

Appendix A

A.1 Conformal Antennas

A.1.1 Introduction

As antennas become miniaturized and the demand for more efficiency increases, it is becoming more difficult for antenna engineers to design antennas that are compact and easily integrated, especially for frequencies in the UHF/VHF bands. A more frequent theme is to use conformal antennas to tackle volume and real estate issues while improving its electrical performance, which can lead to improvements in the overall system performance such as light weight, low power, less signal interference and easy mechanical installation.

IEEE defines conformal antenna as:

An antenna [an array] that conforms to a surface whose shape is determined by considerations other than electromagnetic; for example, aerodynamic or hydrodynamic [7].

Conformal antennas are antennas that are mounted to a surface of an object and follow the shape of the structure. They are an attractive solution for airborne antennas where aerodynamic properties are considered to be crucial performance. In cellular phones, conformal antennas can be placed inside curved surface saving crucial real estate. Their low profile design allows for easy mechanical installation and better electromagnetic performance.

The word ‘conformal’ comes from the Latin word ‘con’ which means together, and ‘formare’ which means to form or to fashion. There have been many studies done on conformal antennas [24], [25], [26], mainly with cylindrical and spherical structures. Although various

types of antennas can conform to a curved surface, patch and slot antennas seem to be the recurring theme due to their low profile.

One of the advantages of conformal antennas is their ability to achieve several geometries. This ability of varying their shape to be adjusted to the contour of different structures improves not only the EM performance, but also mechanical, aerodynamic or hydrodynamic. As they are structurally integrated there is no need for conventional radomes. In addition, their radar cross section (RCS) can be much lower than for their planar counterparts. For some cases, the physical size of certain antennas could be much smaller than in the planar case, for instance the toroidal antenna introduced in [27] , when it is designed for high frequencies is relatively smaller compared to other microstrip antennas of the same frequency range. By varying the shape of conformal antennas, the gain can be controlled, with a nearly omnidirectional coverage while reflections are considerably reduced.

The drawbacks of conformal antennas are design complexity and manufacturing cost. Their physical size is restricted to the environment where they are housed, and designers have to be creative to accommodate packaging the antenna and its system.

First, we introduce the theory of conformal antennas on a singly curved surface and later we simulate a circularly polarized antenna with a dipole-like radiation pattern mounted on a singly curved surface using EMPIRE XPU simulation tool. The performance of the antenna is compared to the performance after being conformed on a curved surface.

A.1.2 Conformal Antennas on Singly Curved Surface

Single curved surfaces are easy to analyze since they can be unfolded and analyzed as a flat surface using two dimensional analysis as shown in 7.1 [24].

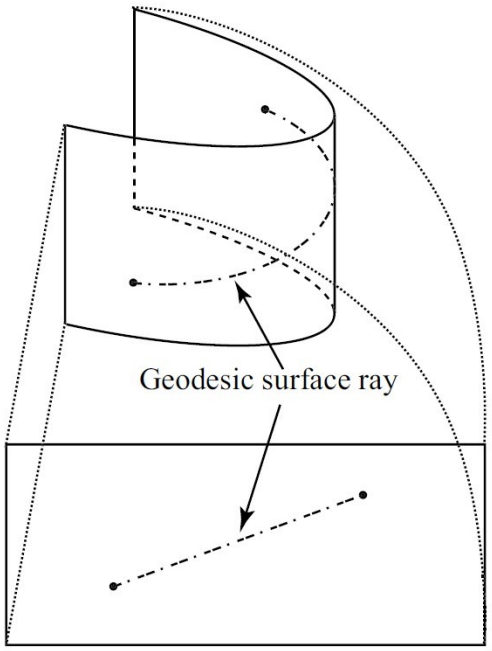

Figure 82: 2D cylindrical surface **[24]**

Geodesics, as shown in Figure 82, are defined as lines of the shortest distance between points on a surface. The equations of geodesics are found from the study of variational problem and is beyond the scope of this topic. The solution to the geodesics equation in its general form is given in [24]. The general expression for a singly curved surface in the geodesic coordinate system is:

$$x = f(u), \qquad y = g(u), \qquad z = v$$

and the geodesic equation for this singly curved surface becomes

$$\frac{dv}{du} = \frac{\alpha\sqrt{\left(f'(u)\right)^2 + \left(g'(u)\right)^2}}{\sqrt{1-\alpha^2}} \tag{48}$$

with the solution

$$v(u) = \frac{\alpha}{\sqrt{1-\alpha^2}} \int \sqrt{\left(f'(u)\right)^2 + \left(g'(u)\right)^2}\, du + \beta = \Im(\mathrm{u}, \alpha) + \beta \qquad (49)$$

The above equation defines all possible geodesics. For a circular cylinder the parametric equations *x, y* and *z* are given in [24] for a singly curved surface as

$$x = a\cos\phi\,, \qquad y = \mathrm{a}\sin\phi\,, \qquad z = z$$

The solution to geodesic equation reduces to

$$v = \frac{\alpha}{\sqrt{1-\alpha^2}}[\alpha u] + \beta \qquad (50)$$

The circular cylinder is often used in conformal antennas for its simple geometry. The dimensions of the cylindrical antennas studied in this section follow the procedure described in [28] and the probe position is found using an iterative process proposed by [29]. The probe must be placed in the specific point that excites the modes TM01 (z-direction excitation) and TM10 (φ-direction excitation) with the same amplitude and 90^o phase difference to produce RHCP. For this, the feeding must be selected in the diagonal of the quasi-square patch [9] so that

$$\frac{z'}{2b} = \frac{l'}{l}$$

where the parameters are illustrated in Figure 83.

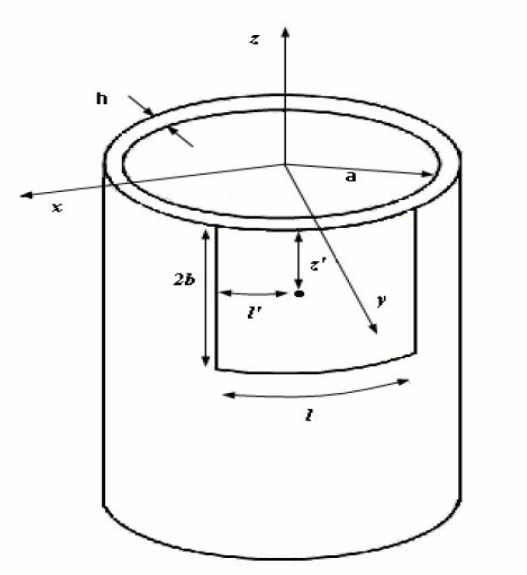

Figure 83: Cylindrical microstrip antenna **[24]**

An approximate value of the resonance frequency can be found by using a planar solution. The resonant frequency for the mnth TM mode is given by [24]:

$$f_{mn} = \frac{c}{s\sqrt{\epsilon_r}}\left[\left(\frac{m}{W}\right)^2 + \left(\frac{n}{W}\right)^2\right]^{\frac{1}{2}} \tag{51}$$

where the effective circumferential length of the patch is given by

$$W = 2R\phi_o + \frac{t}{\sqrt{\epsilon_r}} \tag{52}$$

and the effective axial length is

$$L = z_m + \frac{t}{\sqrt{\epsilon_r}} \tag{53}$$

The actual dimensions of the patch are the terms $2R\phi_o$ and z_m, where

R is the radius of the cylinder

ϕ_o is the angle from the center of the straight edge

z_m is the axial length of the patch

A.1.3 Conformal Antenna on a Curved Surface

The main goal for an antenna mounted on a surface is to maximize the output power by minimizing the reflected power. To explain this further we consider radome theory which suggests that, to reduce attenuation, the radome material should be < 0.1λ while the antenna should be 0.25λ away from the radome material to reduce destructive reflections [30] [31]. While this can be achieved in the microwave band, it is a problem in the UHF/VHF band as the wavelength at these frequencies are in the order of 1-3 meters. Wavelength in a radome material becomes shorter than wavelength in free space (λ_o), depending on the dielectric properties of the radome, and is inversely proportional to the square of the dielectric constant ϵ_r.

$$\lambda = \frac{\lambda_o}{\sqrt{\epsilon_r}} \tag{54}$$

The thickness to obtain optimum electromagnetic transparency is also inversely proportional to the square of the dielectric constant ϵ_r and is given as

$$thickness = \frac{\lambda_o}{2\sqrt{\epsilon_r}} \tag{55}$$

By making the antenna part of the structure housing it, the structure effectively becomes the antenna and the radome effect would be minimized if not completely removed. The electrical properties however must be accounted for to properly tune the antenna to a desired frequency. Properties to consider are mainly the material dielectric constant (ϵ_r), dissipation factor ($\tan\alpha$) and skin thickness.

An experiment was performed to verify this by simulating a circularly polarized antenna with a dipole-like radiation pattern mounted on a curved structure (Figure 84). The dielectric parameters of both the curved structure and the patch antenna were identical except the antenna includes a radiating element (not shown). The relative permittivity

(dielectric constant) was 4.9 with loss tangent of 0.025 and thermal conductivity of 0.256 Watts/ (meter·Kelvin).

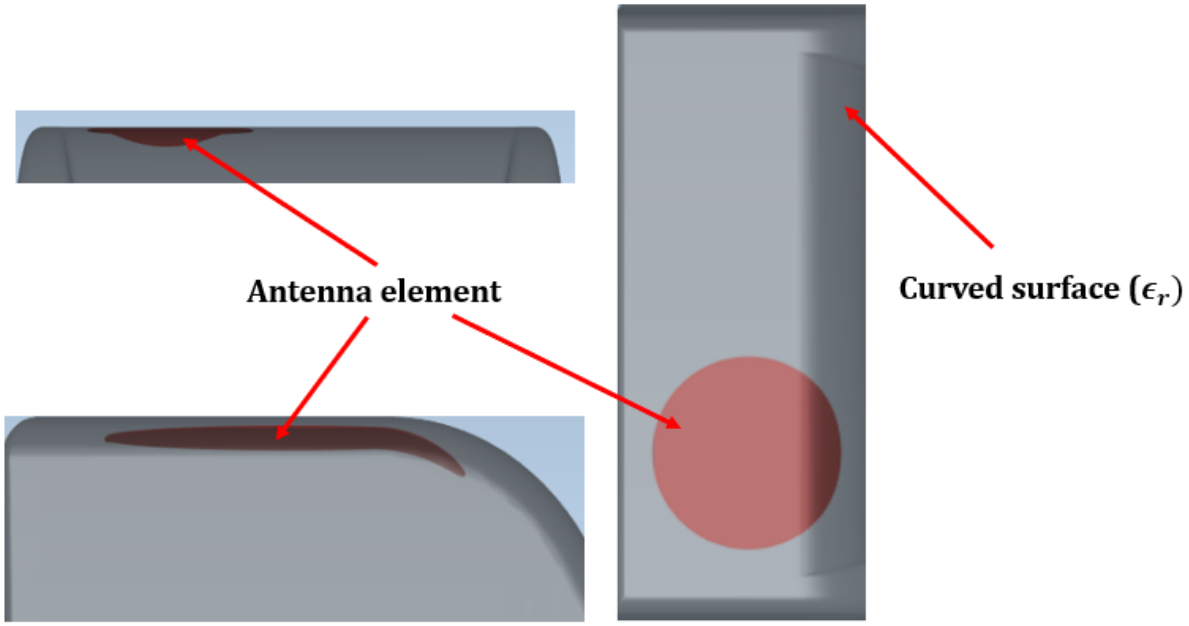

Figure 84: Top and side views of antenna conformed on a curved surface

The circularly polarized antenna performance in free space is compared to its performance after being conformed to a curved structure. Both configurations were simulated on a 2 meter diameter ground plane. The radiation pattern for the circular antenna in free space is shown in Figure 85. The circular antenna used for this simulation is unconventional but cannot be shown due to pending patents. It has a null at the zenith and is approximately omnidirectional in the azimuth plane. This patch antenna was then placed on a curved structure of the same dielectric properties and simulated in an identical manner as the circular antenna; the radiation pattern is shown in Figure 86. Note, in both results, the patch antenna is in its normal position facing up in the z coordinate. The results are interesting in that the radiation pattern now looks more like a typical patch antenna with the null filled at the zenith. This is a remarkable solution especially for ELTs where high elevation beam coverage is a requirement to access satellites in emergency situations.

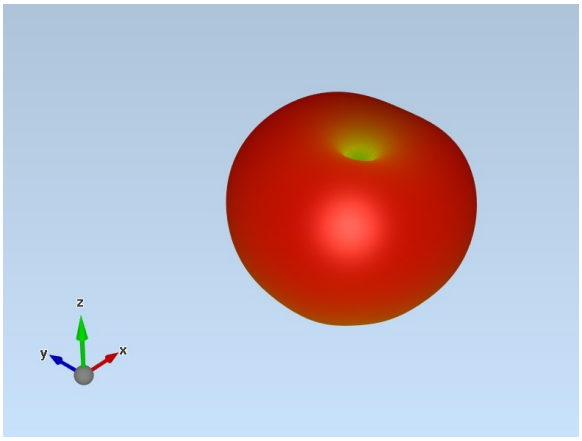

Figure 85: Simulated radiation pattern of circularly polarized antenna

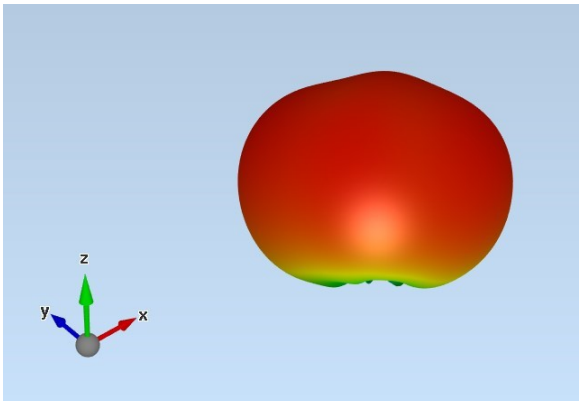

Figure 86: Simulated radiation pattern of circular antenna conformed on a curved structure

Appendix B

B.1 COSPAS/SARSAT System

C/S is a satellite system designed to supply alert and location information to assist search and rescue operations. The Russian “Cospas" translate to “space system for the search of vessels in distress", whilst “Sarsat" stands for “Search and Rescue Satellite-Aided Tracking". The system uses satellites and ground stations to detect and locate signals from ELT operating at frequencies of 406 MHz, 243 MHz and/or 121.5 MHz. It provides worldwide support to organizations responsible for air, sea and ground SAR operations.

The Cospas-Sarsat system consists of three main parts. The first part consists of emergency beacons, sending out a signal when a person or vehicle is in distress. The second part is the space segment that consists of geosynchronous satellites (GEOSARs) and low-earth polar orbit satellites (LEOSARs). The last part is the ground segment consisting of Local User Terminals (LUTs) and Mission Control Centers (MCCs), to process the signals received by the satellites. The LUTs are divided into GEOLUTs and LEOLUTs, depending on the type of satellites they communicate with. Once the ADFR transmits the distress signal pulses, the satellites will process and relay the information from the beacons to the ground segment. The information from the ground segments is then used to coordinate the rescue mission. An overview of this principle is shown in Figure 87.

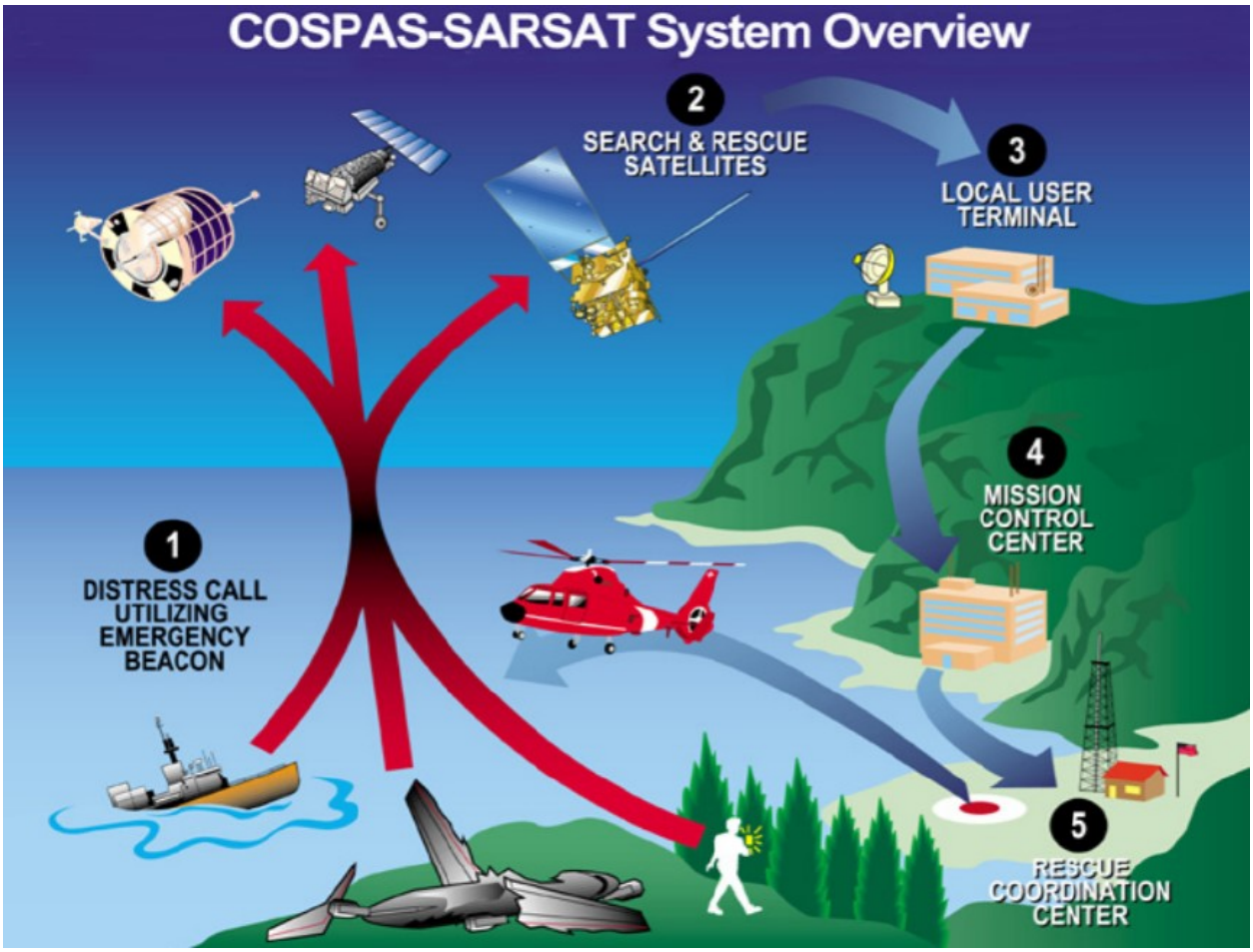

Figure 87: Overview of Cospas-Sarsat system [32]

Originally, only the low-orbit satellites were used to detect distress signals. Using the Doppler location technique, they can determine the origin of a transmitted signal. The downside of their low altitude is a limited field of vision, where the satellite only covers a part of the earth's surface. Therefore, they are not always `visible' to a beacon and a LUT at the same time. When receiving a signal, the module stores it for a short period of time until it is able to relay the data to a LUT. With the earth moving underneath the satellite, it can take 12 hours for a beacon to come within range of the module. Currently, there are six of these satellites in orbit, with five fully functional [33]. This reduces typical waiting time for this process to less than an hour.

The network was expanded in later years with geostationary satellites to enable faster response times. Because the earth does not move in relation to these satellites, they cannot use the Doppler method to determine the location of the beacon, so a location must be sent along with the distress signal. There are currently nine of these satellites of which six are fully operational [34] Currently, C/S is in the process of upgrading its satellite system by placing search-and-rescue receivers (repeaters or transponders) on new GPS satellites operated by the United States, navigation satellites of Russia (GLONASS) that began deployment last year, and European GALILEO navigation satellites that began launching 12 October 2012. Once qualified as operational, this system augmentation will dramatically improve both the speed and location-accuracy for detecting beacons. Those satellites orbit the Earth at an altitude between 19,000 and 24,000 km, a range considered as medium-altitude Earth orbit. Hence this component of Cospas-Sarsat is known as the Medium-altitude Earth Orbit Search and Rescue system, or MEOSAR. It will complement the existing LEOSAR and GEOSAR systems.

Once fully operational, the MEOSAR system will offer the advantages of both LEOSAR and GEOSAR systems without their respective limitations by providing transmission of the distress message, and independent location of the beacon, with a near real time worldwide coverage. It will also facilitate other planned enhancements for Cospas-Sarsat beacons, such as a return link transmission that will allow the beacon to provide to the user a confirmation that the distress message has been received [34] The large number of MEOSAR satellites that will be in orbit when the system is fully operational will allow many distress messages to be relayed at the same time by several satellites to several ground antennas, improving the likelihood of detection and the accuracy of the location determination.

B.2 ELT Board

Figure 88 shows the ELT board which is the transmitter that powers the internal antennas in the ADFR beacon. It transmits C/S radio signals at the 406 MHz frequency band based on First Generation Beacons (FGB) BPSK modulated, and Second Generation Beacons (SGB) spread spectrum OQPSK modulated. It also transmits at 121.5 MHz or 243 MHz frequency bands used for homing on to a deployed beacon. It features an internal GNSS receiver device that receives position data from GNSS satellite constellations. It is temperature and shock hardened and fully compliant to ED-62A.

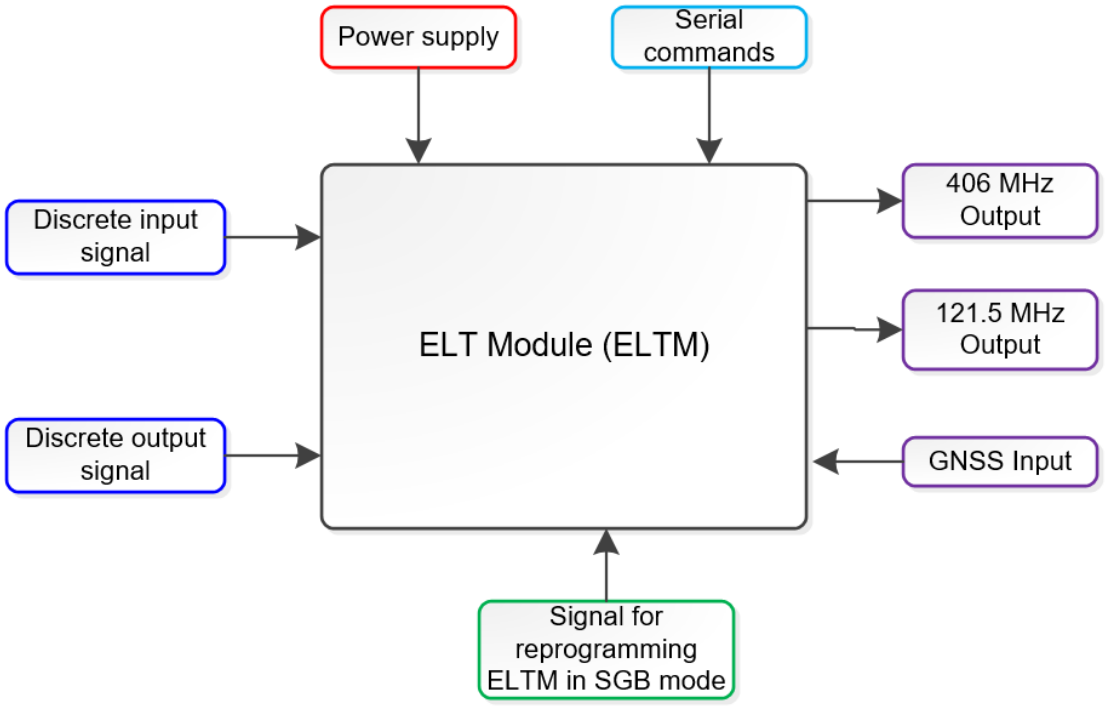

Figure 88: ELT Board Block Diagram

The ELT board is powered by a 9 V lithium battery placed inside the Beacon Airfoil Unit (BAU). The circuit will activate when the ELTM is in proper mode of operation. Low voltage DC-to-DC converter down-converts the battery voltage to 3.3 V and supplies the GNSS and the ELT board, except the

406 MHz and 121.5 MHz antennas. A high voltage DC-to-DC converter is used to down-convert the battery to 8 V to supply the 406 MHz amplifier devices. The 121.5/243 antennas are supplied with 7.2 V providing power up to 0.5 W.

Appendix C

C.1 Antenna Measurement Analysis

To determine the calibration factor of the anechoic chamber, which includes the total cable loss from transmit and receive antennas going to the power measurement device, gain standard-transfer (reference antenna) method is applied. To calculate total radiated power from the AUT, we must determine the EIRP applying the Gain Standard Antenna (GSA), which is a calibrated antenna whose gain is predetermined. It is very critical to determine the characteristics of the calibration antenna by making sure the gain of the GSA is accurately known, choosing an antenna with a stable pattern (omnidirectional) so that a slight orientation does not compromise power readings and a good VSWR response so that it accepts the power delivered to it. To understand the equation of EIRP, we will first introduce Friis transmission equation, which is essential in the analysis and design of wireless communication systems.

C.1.1 Theory

The Friis transmission equation relates the amount of power received (P_{RX}) at the terminals of a receiving antenna, to the amount of power transmitted (P_{TX}) at the terminals of a transmitting antenna where the two antennas are in the far-field of each other, separated by a distance R. Friis transmission equation relating transmitted (reference monopole) and received (log-periodic) power is given as:

$$P_{R_{GSA}} = P_{T_{GSA}} + G_R + G_{T_{GSA}} - L_{tot} \tag{56}$$

where,

$P_{R_{GSA}}$: Power at Receiver from monopole at 10 dBm [dBm]

$P_{T_{GSA}}$: Transmit Power at Gain Standard Antenna (Reference monopole) [dBm]

$G_{T_{GSA}}$: Gain of GSA (monopole) [dBi]

G_R : Receiver Antenna Gain (log periodic) [dBi]

L_{tot} : Total loss [dB]

Here, the total loss is the sum of path loss (cable loss) and polarization misalignment also called Polarization Loss Factor (PLF). We can denote that as,

$$L_{tot} = L_{path} + PLF \tag{57}$$

To obtain maximum power transfer from a transmitter antenna to a receiver antenna, the polarization of the EM waves should be identical and aligned in the same sense. The PLF accounts for power loss due to polarization mismatch. The polarization loss factor between two antennas is given by:

$$PLF = \cos^2(\varphi) \tag{58}$$

where φ is the polarization offset between the two antennas. If the transmit and receive antennas are linearly polarized, then φ = 0 and PLF = 1. On the other hand, if the transmit antenna is linear (vertical or horizontal) and the receiver is a circularly polarized antenna ($RHCP$ or $LHCP$), then φ = 90^0 and PLF = 0.5. Table 6 summarizes the PLF for different antenna polarizations.

Table 6: PLF values for Linear, RHCP and LHCP antennas

Transmit Antenna Polarization	Receive Antenna Polarization	φ	PLF
Linear or Vertical	Linear or Vertical	0◦	1
Linear (V or H)	Circular (RH or LH)	90°	0.5
Vertical	Horizontal	180°	0
RHCP	RHCP	0◦	1
RHCP	LHCP	180°	0

We can re-write Equation 56 as below:

$$L_{tot} = P_{T_{GSA}} + G_R + G_{T_{GSA}} - P_{R_{GSA}} \tag{59}$$

The antenna relationship between the receiver (log-periodic) and the antenna under test (AUT) can similarly be derived using the Friis transmission equation:

$$P_{R_{AUT}} = P_{T_{AUT}} + G_R + G_{T_{GSA}} - L_{tot} \tag{60}$$

where,

$P_{T(AUT)}$: Transmit Power at AUT [dBm]

$P_{R(AUT)}$: Power at Receiver from AUT at 40 dBm [dBm]

$G_{T(AUT)}$: Gain of AUT [dBi]

Since the total loss L_{tot} is given in terms of known variables from the reference monopole, we can insert L_{tot} in Equation 60 to evaluate power received from the AUT:

$$P_{R_{AUT}} = P_{T_{AUT}} + G_{T_{AUT}} - P_{T_{GSA}} + G_{T_{GSA}} - P_{R_{GSA}} \quad (61)$$

Note the G_R term is cancelled out, which means the gain at the receive end is not necessary to obtain the received power of the AUT.

C.1.2 EIRP Computation

The Effective Isotropically Radiated Power (EIRP) is the power ratio of power radiated by an antenna to the power radiated by an ideal (fictitious) isotropic source and is related to the gain of the antenna and the transmitted power at the antenna input terminal. It is given as:

$$EIRP = P_T\,[dBm] + G_T\,[dBi] \quad (62)$$

where, P_T is the transmitted power at the input of the antenna in dBm, and G_T is the gain of the antenna in dBi.

To calculate the EIRP of the antenna under test from Equation 61, we can rearrange it in this format:

$$P_{T_{AUT}} + G_{T_{AUT}} = P_{R_{AUT}} + P_{T_{GSA}} + G_{T_{GSA}} - P_{R_{GSA}} \quad (63)$$

EIRP is then simply expressed as:

$$EIRP = P_{T_{AUT}} + G_{T_{AUT}} \quad (64)$$

C.1.3 Antenna Calibration

A quarter-wave monopole antenna with a gain of 0.5 dBi is used to calibrate antenna transmitting at 406 MHz and positioned on the transmit side, while a log-periodic antenna is used as a receiver in the shielded anechoic chamber. Two sets of measurements were recorded with two antenna configurations. The first measurement was taken by transmitting a 10 mW power through the reference monopole at 406 MHz, and the received output signal power is received by the log-periodic antenna and values recorded by the spectrum analyzer. Table 7 shows the values obtained between transmitter (monopole) and receiver (log-periodic) antennas.

Table 7: Reference monopole measured values

Receive Antenna Type	**Log-periodic**
Transmit Antenna Type	$\frac{\lambda}{4}$ monopole (406 MHz)
Transmit Power, $P_{T(GSA)}$ [dBm]	10 mW
Receive Power, $P_{R(GSA)}$ [dBm]	-28 dBm
Reference Monopole Gain, $G_{T(GSA)}$ [dBi]	0.5 dBi

The second measurement was taken with the same log-periodic antenna setup as receiver while the AUT was transmitting at 10 mW. Note the gain of the AUT is unknown.

Table 8: Measured values of AUT

Receive Antenna Type	Log-periodic
Transmit Antenna Type	AUT
Transmit Power, $P_{T(GSA)}$ [dBm]	10 mW
Receive Power, $P_{R(GSA)}$ [dBm]	-
Gain of AUT, $G_{T(GSA)}$ [dBi]	unknown

From Equation 60 we can evaluate the power received from a reference monopole at a given transmit power of 10 dBm. The antenna gain of the monopole is known to be 0.5 dBi (at an elevation angle of 10˚). Note, the gain of antenna is not constant throughout the vertical cut and elevation angle should be specified when quoting gain of a monopole. The horizontal cut of a monopole over a perfectly conducting ground plane is omnidirectional, hence the difference in gain in the azimuth direction should be considered negligible.

Finally, using values obtained in Table 7 and Table 8, the EIRP for the antenna under test can be obtained.

Appendix D

Python Script for Vivaldi Antenna Conformed on a Cylinder

```
from math import * import
numpy as np

def vivaldigeom(pts in, args):
    #-- Input from EMPIRE --
      X0 = ptsin [0][0]                          # First input point, x-coordinate
      Y0 = pts_in [0][1]                         # First input point, y-coordinate
    X1 = 1e-6 * (ptsin[1][0] - X0) # Second input point, x-coordinate
    Y1 = 1e-6 * (ptsin[1][1] - Y0) # Second input point, y-coordinate
    X2 = 1e-6 * (ptsin[2][0] - X0) # Third input point, x-coordinate
    Y2 = 1e-6 * (ptsin[2][1] - Y0) # Third input point, y-coordinate
    R  = max(1,float(args[0])) # Radius, defined as first argument in userpoly textbox
     npb = 300                                   # Number of output-points to describe bow

    #-- coefficient-calculation --
    a = (Y2 - Y1) / (exp(R*X2) - exp(R*X1))
    b = (Y1*exp(R*X2) - Y2*exp(R*X1)) / (exp(R*X2) - exp(R*X1))

    #-- output-polygon-calculation --
    pts out = [] # empty list of output-points (2D-polygon-coodinates) for x in
    np.arange(0, X2, X2/npb): x = float(x) y = float(b + a*exp(R*x)) pts _
    out.append((X0+1e6*x, Y0+1e6*y)) # successively fill up 2D-
    polygon-coodinate-list
```

```
pts out.append((X0+1e6*X2, Y0+1e6*Y2)) # add end−point pts out.append((X0+1e6*X1, Y0+1e6*Y2)) # add
corner−point

    #−− return −− return pts out # return 2D−polygon−coodinate−list to
    EMPIRE



#
    −−−−−−−−−−−−−−−−−−−−−−−−−−−−−−−−−−−−−−−−−−−−−−−−−−−−−−


import Numeric


class
    cylinder:
    """

        2d coordinate transformation for
        cylinder coordinates


        x−axis: azimuth, length invariant at z=zref
        z−axis: radius y−axis: unchanged

    """
    #
    # Needed from outside

#
dir = 1            #        Direction to be constant, x:0, y:1, z:2
reso = 5000.0      #              GL−Resolution (high values: coarse, low values: fine)

#
# Inside definitions
#
dr      = 2           #   Radius direction:        here z
dphi    = 0           #   Azimuth direction: here x
```

```
rref      = 1570.0          #          Reference r−coordinate (no stretching in phi−dir)

r0        = −20000.0        #          Center r−coordinate
phi0      = −1280.0         #          Center phi−coordinate
  def transform(s,p0):
        "Do coordinate transformation dir+1,dir+2"

        rad             = (p0[s.dr      ]−s.r0     )
        ang               = (p0[s.dphi]−s.phi0)/(s. rref−s.r0)

        p1  = Numeric.array(p0).copy() p1[s.dr]        = s.r0     + rad ∗
        Numeric.cos(ang) p1[s.dphi] = s.phi0 + rad ∗ Numeric.sin(ang)

        return p1

  def back(s,p0):
        "Inverse coordinate transformation" rr          = p0[s.dr
            ]−s.r0 pp           = p0[s.dphi]−s.phi0

            rad       = sqrt(rr∗rr+pp∗pp)

      ang               = atan2(pp,rr)

      p1                = Numeric.array(p0).copy()

      p1[s.dr]          = s.r0          + rad
      p1[s.dphi]        = s.phi0 + ang∗(s.rref−s.r0)

        return p1
```